



FEDERAL UNIVERSITY OF PARÁ
GEOSCIENCES INSTITUTE
POST-GRADUATE PROGRAM IN GEOPHYSICS

MASTER'S DISSERTATION

**Local anisotropy estimation from VSP data: analysis
of 3D survey design**

BRUNO DOS SANTOS SILVA

Belém
2018

BRUNO DOS SANTOS SILVA

**Local anisotropy estimation from VSP data: analysis
of 3D survey design**

Master's dissertation submitted to the Post-Graduate
Program in Geophysics of the Federal University of Pará
for obtaining a Master's Degree in Geophysics.

Concentration area: Seismic Methods

Advisor: Dr. Ellen de Nazaré Souza Gomes

Belém
2018

Dados Internacionais de Catalogação-na-Publicação (CIP)
Biblioteca do Instituto de Geociências/SIBI/UFPA

Silva, Bruno dos Santos, 1992-

Local anisotropy estimation from VSP data: analysis of 3D survey design / Bruno dos Santos Silva. – 2018

46 f. : il. ; 30 cm

Inclui bibliografias

Orientadora: Ellen de Nazaré Souza Gomes

Dissertação (Mestrado) – Universidade Federal do Pará, Instituto de Geociências, Programa de Pós-Graduação em Geofísica, Belém, 2018.

1. Inversão (Geofísica). 2. Anisotropia. 3. Perfilagem sísmica vertical. I. Título.

CDD 22. ed.: 550

Elaborado por
Hélio Braga Martins
CRB-2/698

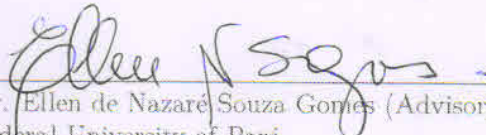
BRUNO DOS SANTOS SILVA

Local anisotropy estimation from VSP data: analysis of 3D
survey design

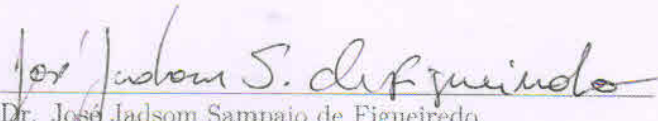
Master's dissertation submitted to the Post-Graduate
Program in Geophysics of the Federal University of Pará
for obtaining a Master's Degree in Geophysics.

Approval Date: March 27, 2018

Committee Members:



Dr. Ellen de Nazare Souza Gomes (Advisor)
Federal University of Pará



Dr. Jose Jadsom Sampaio de Figueiredo
Federal University of Pará



Dr. Amin Bassrei
Federal University of Bahia

Aos meus pais Silvia e Sebastião.
Ao meu avô Evandro (in memoriam).

ACKNOWLEDGMENTS

Agradeço à minha orientadora, professora Ellen Gomes, pela orientação ao longo da elaboração deste trabalho, pela oportunidade e confiança depositada em mim ao longo do meu percurso acadêmico.

Ao professor Ivan Pšenčík pelas importantes discussões e por disponibilizar o software ANRAY.

À Zoraida Tejada por sua ajuda na fase inicial deste trabalho.

Aos professores Amin Bassrei e José Jadsom Sampaio de Figueiredo pela participação na banca examinadora.

Aos professores do Programa de Pós-graduação em Geofísica e da Faculdade de Geofísica pela contribuição na minha formação acadêmica.

A CAPES pelo suporte financeiro.

RESUMO

Os dados de vagarosidade e polarização da onda qP obtidos em experimento VSP (Vertical seismic profile) possibilitam estimar a anisotropia na vizinhança de um geofone localizado no interior do poço. Utilizando a teoria da perturbação, um meio fracamente anisotrópico pode ser modelado a partir de uma perturbação de primeira ordem entorno de um meio isotrópico de referência. O esquema de inversão baseia-se em uma aproximação linear em que os dados de vagarosidade e polarização são expressos em termos dos parâmetros WA (weak anisotropy). Este parâmetros caracterizam o desvio do meio anisotrópico a partir do meio isotrópico de referência. No esquema de inversão apresentado, utiliza-se as três componentes da polarização, pois considera-se receptores 3C (três-componentes), e apenas uma das componentes de vagarosidade, aquela na direção do poço onde está o arranjo dos receptores. Logo, o método sofre influência da orientação do poço. Neste trabalho, estudamos o desenho de experimentos VSP multiazimutal, levando em conta diferentes tipos de distribuições de fontes na superfície e a configuração do poço, isto é, considerando os receptores no interior de um poço vertical e horizontal. Os testes numéricos foram realizados para um meio anisotrópico heterôgeneo com simetria transversalmente isotrópica com eixo inclinado. Os resultados mostraram que os parâmetros WA que são determinados com acurácia dependem da orientação do poço e ainda considera-se que a velocidade de fase da onda qP é bem estimada em uma região delimitada por um cone de 30° entorno da direção do poço.

Palavras-chaves: Fraca anisotropia. Anisotropia local. Inversão linear. VSP multiazimutal. Poço horizontal.

ABSTRACT

Measurements of slowness and polarization of qP -wave obtained from VSP (vertical seismic profile) experiments allow estimating the anisotropy in the vicinity of a borehole geophone. Using the perturbation theory, a weakly anisotropic medium can be modelled by first-order perturbation around an isotropic reference medium. The inversion scheme is based on a linear approximation which expresses the slowness and polarization in terms of WA (weak anisotropy) parameters. These parameters characterize the deviations of the anisotropic medium from a reference isotropic medium. In presented inversion scheme, we use the three components of the polarization, since we consider 3C (three-components) geophones, and only one of the slowness components, the one along the wellbore direction, where is located the receiver array. Thus, it depends on the wellbore orientation. In this work, we study the survey design of VSP experiments, taking into account different sources distributions on the surface and the wellbore configuration, that is, considering the vertical and horizontal borehole. The numerical experiments are performed for a heterogeneous transversely isotropic medium with the tilted symmetry axis (TTI). The inversion results showed that the WA parameters which are accurately determined depends on the wellbore orientation, further it is consider that the qP -wave phase velocities can be well estimated within a 30° cone around the borehole direction.

Keywords: Weak anisotropy. Local anisotropy. Linear inversion. VSP multiazi-muthal. Horizontal well.

LIST OF FIGURES

3.1	Schematic illustration of models with receiver in vertical and horizontal borehole. The first layer (ANI) is heterogeneous anisotropic and the second one (ISO) is homogeneous isotropic. (a) Vertical borehole with receivers in the direction of the z -axis. (b) Horizontal borehole with receivers parallel to the x -axis direction.	10
3.2	Plan view of the acquisition geometries used in the numerical tests. Three types of source distribution are considered: five radial profiles (with angular steps of 72°), randomly and spiral pattern. 90 sources are used in VSP experiments with vertical borehole configuration (Fig.3.2a, Fig.3.2c and Fig.3.2e). For VSP experiments with horizontal borehole configuration, 180 sources are employed (Fig.3.2b, Fig.3.2d and Fig.3.2f).	12
3.3	Singular values for the three acquisition geometries (see Figure 3.2) of VSP experiments with vertical borehole. The vertical axes are in logarithmic scale. (a) Result for sources along five profiles. (b) Result for sources randomly distributed. (c) Result for sources in spiral pattern.	14
3.4	Model resolution matrix for the three acquisition geometries of VSP experiments with vertical borehole is equal to identity matrix, which means that all 15 parameters can be uniquely determined.	15
3.5	Singular values for the three acquisition geometries (see Figure 3.2) of VSP experiments with horizontal borehole. The vertical axes are in logarithmic scale. (a) Result for sources along five profiles. (b) Result for sources randomly distributed. (c) Result for sources in spiral pattern.	15
4.1	Estimated velocities of the reference isotropic medium to the receiver 1 of the vertical borehole. The estimation is based on Eq. 2.21 and uses the components of the slowness and polarization along z -axis of the direct and reflected wave. Results for the three acquisition geometries: (a) sources along 5 profiles, (b) random sources, (c) spiral sources pattern.	18
4.2	Model covariance matrices computed for experiments using the three acquisition geometries to the receiver 1 of the vertical borehole. (a) For sources along 5 profiles. (b) For random sources. (c) For spiral sources pattern.	19

4.3	Stereographic maps to the receiver 1 of the vertical borehole. (a) Phase velocity computed using exact WA parameters. (b) Phase velocity computed using estimated WA parameter for experiment with sources distributed along five profiles. (c) Phase velocity computed using estimated WA parameter for experiment with sources distributed randomly. (d) Phase velocity computed using estimated WA parameter for experiment with sources distributed in spiral pattern. (e) Percentage error between (a) and (b). (f) Percentage error between (a) and (c). (g) Percentage error between (a) and (d).	20
4.4	Percentage variation maps (stereographic projections and its corresponding spherical surfaces) of phase velocity to the receiver 1 of the vertical borehole. (a) Results for sources along 5 profiles. (b) Results for sources distributed randomly. (c) Results for sources distributed in spiral pattern.	21
4.5	Estimated velocities of the reference isotropic medium to the receiver 2 of the vertical borehole. The estimation is based on Eq. 2.21 and uses the components of the slowness and polarization along z-axis of the direct and reflected wave. Results for the three acquisition geometries: (a) sources along 5 profiles, (b) random sources, (c) spiral sources pattern.	22
4.6	Model covariance matrices computed for experiments using the three acquisition geometries to the receiver 2 of the vertical borehole. (a) For sources along 5 profiles. (b) For random sources. (c) For spiral sources pattern. . .	23
4.7	Stereographic maps to the receiver 2 of the vertical borehole. (a) Phase velocity computed using exact WA parameters. (b) Phase velocity computed using estimated WA parameter for experiment with sources distributed along five profiles. (c) Phase velocity computed using estimated WA parameter for experiment with sources distributed randomly. (d) Phase velocity computed using estimated WA parameter for experiment with sources distributed in spiral pattern. (e) Percentage error between (a) and (b). (f) Percentage error between (a) and (c). (g) Percentage error between (a) and (d).	24
4.8	Percentage variation maps (stereographic projections and its corresponding spherical surfaces) of phase velocity to the receiver 2 of the vertical borehole. (a) Results for sources along 5 profiles. (b) Results for sources distributed randomly. (c) Results for sources distributed in spiral pattern.	25
4.9	Estimated velocities of the reference isotropic medium to the receiver in the horizontal borehole. The estimation is based on Eq. 2.21 and uses the components of the slowness and polarization along x-axis of the direct wave. Results for the three acquisition geometries: (a) sources along 5 profiles, (b) random sources, (c) spiral sources pattern.	26

4.10	Model covariance matrices computed for experiments using the three acquisition geometries to the receiver in the horizontal borehole. (a) For sources along 5 profiles. (b) For random sources. (c) For spiral sources pattern. . .	27
4.11	Stereographic maps to the receiver in the horizontal borehole. (a) Phase velocity computed using exact WA parameters. (b) Phase velocity computed using estimated WA parameter for experiment with sources distributed along five profiles. (c) Phase velocity computed using estimated WA parameter for experiment with sources distributed randomly. (d) Phase velocity computed using estimated WA parameter for experiment with sources distributed in spiral pattern. (e) Percentage error between (a) and (b). (f) Percentage error between (a) and (c). (g) Percentage error between (a) and (d).	28
4.12	Percentage variation maps (stereographic projections and its corresponding spherical surfaces) of phase velocity to the receiver in the horizontal borehole. (a) Results for sources along 5 profiles. (b) Results for sources distributed randomly. (c) Results for sources distributed in spiral pattern.	29

SUMMARY

1	INTRODUCTION	1
2	METHODOLOGY	3
2.1	EQUATIONS FOR THE WEAK-ANISOTROPY (WA) PARAMETERS .	5
2.1.1	Formulation for vertical wellbore	5
2.1.2	Formulation for horizontal wellbore	6
2.2	DETERMINATION OF THE REFERENCE MEDIUM PARAMETERS .	6
2.3	INVERSION SCHEME	7
3	EXPERIMENTAL DESIGN	9
3.1	MODEL AND CONFIGURATION OF EXPERIMENTS	9
3.2	SENSITIVITY STUDY	13
4	INVERSION TESTS	17
4.1	INVERSION RESULTS FOR VERTICAL BOREHOLE	17
4.2	INVERSION RESULTS FOR HORIZONTAL BOREHOLE	25
5	DISCUSSION	30
6	CONCLUSION	32
	REFERENCES	34

1 INTRODUCTION

Information about the anisotropy of the subsurface is necessary for a accurate seismic imaging and reservoir characterization. Vertical seismic profile (VSP) data can be used for estimation of local (in-situ) anisotropy with the spatial resolution close to the dominant seismic wavelength (Tsvankin and Grechka, 2011).

Several techniques for estimation of anisotropy parameters from VSP data are found in the literature. In general terms, they can be categorized into two groups: methods that use only slownesses (Gaiser, 1990; Miller and Spencer, 1994; Jílek et al., 2003) and methods that use polarization (direction of particle motion) and slowness (Parscau, 1991; Horne and Leaney, 2000; Dewangan and Grechka, 2003; Grechka and Mateeva, 2007). The application of each method depends primarily on the structural complexities in the overburden. The first group requires the assumption of lateral homogeneity of the overburden. The second one is independent of overburden complexity (Asgharzadeh et al., 2013).

Using first-order perturbation theory, Zheng and Pšenčík (2002) proposed a linearized model that relates perturbations of slowness and polarization of qP -wave to anisotropy parameters in weakly anisotropy media. Gomes et al. (2004) apply this approach to real VSP data collected in the Java Sea region. This method does not depend of structural complexities in the overburden.

According to Rusmanugroho and McMechan (2012), each technique of anisotropy estimation from VSP data are limited somehow by factors such as the survey geometry, data apertures, the wave types, noise level or the model parametrization. Thus, these factors have important implications in experiment design since they directly affects the capability of parameter recovery. Some recent studies have been concerned with analyzing and investigating these relations (Rusmanugroho and McMechan, 2012; Barreto et al., 2013; Macambira et al., 2014; Ruzek and Pšenčík, 2016).

The design of VSP survey will define the illumination of the medium, hence, the information content in the data. Barreto et al. (2013), using the method of Zheng and Pšenčík (2002), investigated the design of multiazimuth walkaway surveys and showed that at least five source profiles are required so that all anisotropy parameters related to qP -wave are independent in the inversion scheme. Recently, Ruzek and Pšenčík (2016), using a method that estimates the anisotropic parameters from P -wave traveltimes, showed that for this approach the use of sources distributed randomly on the surface improves substantially the parameter estimation.

Given the importance of acquisition geometry, in this work, we extend the analysis about survey design presented in Barreto et al. (2013) for other types of multiazimuth (3D) VSP surveys. A common geometry employed in marine acquisitions consists of spiral source pattern. Another interesting geometry is the randomly distribution of sources, as

pointed out by Ruzek and Pšenčík (2016). Thus, we study the use of sources distributed in spiral pattern and randomly on the surface for inversion approach of Zheng and Pšenčík (2002).

On the above studies, the anisotropy estimation is performed for data recorded in vertical wellbore. In this work we also investigate the problem of parameter estimation in a horizontal wellbore. In this situation, it is only possible to measure directly the horizontal component of slowness in the well direction.

Based on methodology of Zheng and Pšenčík (2002), we derived a linearized model which can be used for inversion of VSP data recorded in horizontal wellbore. Additionally, inversion tests with synthetic data are performed and the quality of estimated parameters is evaluated. As horizontal wellbore are commonly drilled in unconventional reservoirs, this work can be useful in studies for this kind of reservoirs such as characterization of fracture and fluid content evaluation.

This work has a format of article. For this reason, the length of this dissertation is reduced in order to help the subsequent submission. Its structure is described in the following. The Chapter 2 presents the linear equation models that relates the anisotropy parameters to VSP data and describes the inversion procedure for local anisotropy estimation. In the Chapter 3 is described: the anisotropic model used in the tests, the VSP survey geometries which are investigated and the procedures for sensitivity analysis with respect to the survey geometry. In Chapter 4 the results of numerical tests for inversion scheme are shown. Chapter 5 discuss the inversion results and the influence of survey design in the parameters estimation. Finally, the Chapter 6 presents the major conclusions about this study.

2 METHODOLOGY

The assumption of weak anisotropy is valid for many situations in exploration geophysics (Thomsen, 1986). According to Farra and Pšenčík (2003), perturbation theory is a useful tool for study of wave properties in weakly anisotropic media. Here, weak anisotropy medium is modeled by first-order perturbations around an isotropic reference medium.

In the following, component notation is used for vectors and matrices. Einstein summation convention is applied to repeated indices. The Cartesian coordinate system (x, y, z) is used for description of the model. The z -axis is chosen positive downwards and the positive x - and y -axes are chosen so that the coordinate system is right-handed.

Let us consider a weakly anisotropic medium and take an isotropic medium as a reference one. The slowness vector p_i of the qP -wave in a weakly anisotropic medium can be expressed as

$$p_i = p_i^0 + \Delta p_i \quad (2.1)$$

or

$$p_i = p_i^0 + \Delta\xi \vec{i} + \Delta\zeta \vec{j} + \Delta\eta \vec{k} = (\xi + \Delta\xi) \vec{i} + (\zeta + \Delta\zeta) \vec{j} + (\eta + \Delta\eta) \vec{k}, \quad (2.2)$$

where p_i^0 is a slowness vector in the reference isotropic medium and Δp_i is its perturbation. \vec{i} , \vec{j} , \vec{k} are unit vectors along the axes x , y and z , respectively. ξ , ζ and η denote projection of the slowness vector p_i^0 onto \vec{i} , \vec{j} , \vec{k} , respectively. $\Delta\xi$, $\Delta\zeta$ e $\Delta\eta$ denote perturbations of p_i^0 . The vector p_i^0 is given by

$$p_i^0 = \alpha^{-1} n_i \quad (2.3)$$

and its components has the form

$$\xi = \frac{n_1}{\alpha}, \quad \zeta = \frac{n_2}{\alpha}, \quad \eta = \frac{n_3}{\alpha}, \quad (2.4)$$

where α is the P -wave velocity and the vector $n_i = (n_1, n_2, n_3)$ represents the wave normal, both in the isotropic reference medium.

The wave normal and polarization vector of the P -wave are identical in an isotropic medium. Thus the polarization vector g_i of qP -wave in a weakly anisotropic can be written as

$$g_i = n_i + \Delta g, \quad (2.5)$$

where Δg is the deviation from the orientation of the polarization vector in a reference isotropic medium.

Let us introduce in the reference isotropic medium three mutually perpendicular unit vectors $e_i^{(1)}$, $e_i^{(2)}$ and $e_i^{(3)}$ so that the vector $e_i^{(3)}$ is identical with the wave normal of the

P -wave n_i . A practical choice of vectors $e_i^{(1)}$ and $e_i^{(2)}$ expressed in terms of components of the vector $e_i^{(3)}$ is as follows (Pšenčík and Gajewski, 1998):

$$e^{(1)} = D^{-1}(n_1 n_3, n_2 n_3, n_3^2 - 1), \quad e^{(2)} = D^{-1}(-n_2, n_1, 0), \quad e^{(3)} = n = (n_1, n_2, n_3), \quad (2.6)$$

where

$$D = \sqrt{n_1^2 + n_2^2}, \quad n_1^2 + n_2^2 + n_3^2 = 1. \quad (2.7)$$

Using the vectors $e_i^{(k)}$, Pšenčík and Gajewski (1998) defined the weak anisotropy matrix:

$$B_{mn} = a_{ijkl} e_i^{(m)} e_j^{(3)} e_l^{(3)} e_k^{(n)} - c_0^2 \delta_{mn}, \quad (2.8)$$

where a_{ijkl} denotes the tensor of density-normalized elastic parameters, c_0 stands for the phase velocity of the reference isotropic medium, specified by the P - and S -wave velocities α and β . For $m = n = 3$, $c_0 = \alpha$; for $m = n = 1$ or 2 , $c_0 = \beta$. The elements of the matrix B_{mn} are linear function of weak anisotropy (WA) parameters. The WA parameters represent a generalization of Thomsen's parameters to anisotropic media of arbitrary symmetry and orientation (Pšenčík and Gajewski, 1998; Farra and Pšenčík, 2003). Propagation of qP -wave in weakly anisotropic medium is specified by 15 WA parameters, which are related to density-normalized elastic parameters in the Voigt notation $A_{\alpha\beta}$ in the following way:

$$\begin{aligned} \epsilon_x &= \frac{A_{11} - \alpha^2}{2\alpha^2}, & \epsilon_y &= \frac{A_{22} - \alpha^2}{2\alpha^2}, & \epsilon_z &= \frac{A_{33} - \alpha^2}{2\alpha^2}, \\ \delta_x &= \frac{A_{13} + 2A_{55} - \alpha^2}{\alpha^2}, & \delta_y &= \frac{A_{23} + 2A_{44} - \alpha^2}{\alpha^2}, & \delta_z &= \frac{A_{12} + 2A_{66} - \alpha^2}{\alpha^2}, \\ \chi_x &= \frac{A_{14} + 2A_{56}}{\alpha^2}, & \chi_y &= \frac{A_{25} + 2A_{46}}{\alpha^2}, & \chi_z &= \frac{A_{36} + 2A_{45}}{\alpha^2}, \\ \epsilon_{15} &= \frac{A_{15}}{\alpha^2}, & \epsilon_{16} &= \frac{A_{16}}{\alpha^2}, & \epsilon_{24} &= \frac{A_{24}}{\alpha^2}, \\ \epsilon_{26} &= \frac{A_{26}}{\alpha^2}, & \epsilon_{34} &= \frac{A_{34}}{\alpha^2}, & \epsilon_{35} &= \frac{A_{35}}{\alpha^2}. \end{aligned} \quad (2.9)$$

The slowness and polarization vectors of a qP -wave propagating in an arbitrary anisotropic medium are linearly related to the WA parameters of this medium through the equations (Zheng and Pšenčík, 2002):

$$B_{K3} = (\alpha^2 - \beta^2)(g_i e_i^{(K)} - \alpha \Delta \xi e_1^{(K)} - \alpha \Delta \zeta e_2^{(K)} - \alpha \Delta \eta e_3^{(K)}), \quad K = 1, 2 \quad (2.10)$$

$$B_{33} = -2\alpha^4 \xi \Delta \xi - 2\alpha^4 \zeta \Delta \zeta - 2\alpha^4 \eta \Delta \eta. \quad (2.11)$$

The symbols B_{13} , B_{23} and B_{33} in Equations 2.10 and 2.11 are elements of the weak anisotropy matrix B_{mn} , which depend on 15 qP -wave WA parameters. These elements

are written in the following form (Pšencík and Gajewski, 1998):

$$\begin{aligned}
B_{13} = & \alpha^2 D^{-1} \left\{ 2\epsilon_z n_3^5 + n_3^4 (\epsilon_{34} n_2 + \epsilon_{35} n_1) + n_3^3 (\delta_x n_1^2 + \delta_y n_2^2 + 2\chi_z n_1 n_2 - 2\epsilon_z) \right. \\
& + n_3^2 \left[(4\chi_x - 3\epsilon_{34}) n_1^2 n_2 + (4\chi_y - 3\epsilon_{35}) n_1 n_2^2 + (4\epsilon_{15} - 3\epsilon_{35}) n_1^3 \right. \\
& + (4\epsilon_{24} - 3\epsilon_{34}) n_2^3 \left. \right] + n_3 \left[(2\delta_z - \delta_x - \delta_y) n_1^2 n_2^2 + 2(2\epsilon_{16} - \chi_z) n_1^3 n_2 \right. \\
& + (2\epsilon_{26} - \chi_z) n_1 n_2^3 + (2\epsilon_x - \delta_x) n_1^4 + (2\epsilon_y - \delta_y) n_2^4 \left. \right] - \chi_x n_1^2 n_2 \\
& \left. - \chi_y n_1 n_2^2 - \epsilon_{15} n_1^3 - \epsilon_{24} n_2^3 \right\}, \quad (2.12)
\end{aligned}$$

$$\begin{aligned}
B_{23} = & \alpha^2 D^{-1} \left\{ n_3^3 (\epsilon_{34} n_1 - \epsilon_{35} n_2) + n_3^2 \left[(\delta_x + \delta_y) n_1 n_2 + \chi_z n_1^2 - \chi_z n_2^2 \right] \right. \\
& + n_3 \left[(2\chi_y - 3\epsilon_{15}) n_1^2 n_2 - (2\chi_x - 3\epsilon_{24}) n_1 n_2^2 + \chi_x n_1^3 - \chi_y n_2^3 \right] \\
& + (\delta_z - 2\epsilon_x) n_1^3 n_2 + (2\epsilon_y - 2\delta_z) n_1 n_2^3 + 3(\epsilon_{26} - \epsilon_{16}) n_1^2 n_2^2 \\
& \left. + \epsilon_{16} n_1^4 - \epsilon_{26} n_2^4 \right\}, \quad (2.13)
\end{aligned}$$

$$\begin{aligned}
B_{33} = & 2\alpha^2 \left\{ \epsilon_z n_3^4 + 2n_3^3 (\epsilon_{34} n_2 + \epsilon_{35} n_1) + n_3^2 (\delta_x n_1^2 + \delta_y n_2^2 + 2\chi_z n_1 n_2) \right. \\
& 2n_3 (\chi_x n_1^2 n_2 + \chi_y n_1 n_2^2 + \epsilon_{15} n_1^3 + \epsilon_{24} n_2^3) + \epsilon_x n_1^4 + \delta_z n_1^2 n_2^2 + \epsilon_y n_2^4 \\
& \left. + 2\epsilon_{16} n_1^3 n_2 + 2\epsilon_{26} n_1 n_2^3 \right\}. \quad (2.14)
\end{aligned}$$

2.1 EQUATIONS FOR THE WEAK-ANISOTROPY (WA) PARAMETERS

Equations 2.10 and 2.11 state a linear relation between the WA parameters of the medium and the polarization vector and perturbations $\Delta\xi$, $\Delta\zeta$ and $\Delta\zeta$ of slowness. Thus this set of equations can be used for inversion of three-component (3C) data recorded in a receiver inside the wellbore.

In VSP surveys with 3C borehole receivers we can determine all components of polarization. Nonetheless the availability of slowness components depends on the complexity of overburden and the borehole orientation. For data acquired under a structurally complex overburden we can only directly determine the slowness component in the direction of receiver array, this is done taking the derivative of the traveltimes with respect to the coordinate of receivers.

2.1.1 Formulation for vertical wellbore

Let us consider a VSP experiment with receivers in a vertical borehole and assume a laterally heterogeneous overburden. In this scenario, we have available only the z -component of the slowness vector, which is represented by $p_3 = \eta + \Delta\eta$. If none of the perturbations $\Delta\xi$ and $\Delta\zeta$ is known we can obtain the equation for inversion by eliminating these perturbations from Equations 2.10 and 2.11. Eliminating initially $\Delta\xi$ we obtain the

set of equations:

$$\xi (\alpha^2 - \beta^2)^{-1} B_{K3} - \frac{1}{2} \alpha^{-3} B_{33} e_1^{(K)} = \xi g_i e_i^{(K)} - \alpha \Delta \zeta - \alpha \Delta \eta (\xi e_3^{(K)} - \eta e_1^{(K)}), K = 1, 2, \quad (2.15)$$

where

$$X^{(K)} = \xi e_2^{(K)} - \zeta e_1^{(K)}, \quad (2.16)$$

then we eliminate $\Delta \zeta$ from Equation 2.15 and rearrange it in such way that we find the following form:

$$D(\alpha^2 - \beta^2)^{-1} B_{13} - \frac{1}{2} \alpha^{-1} B_{33} \eta = D g_i e_i^{(1)} + \alpha \Delta \eta. \quad (2.17)$$

This formulation is used in the studies of Gomes et al. (2004), Barreto et al. (2013) and Macambira et al. (2014) for estimation of WA parameters.

2.1.2 Formulation for horizontal wellbore

We now consider a VSP survey with receivers in a horizontal borehole along x -axis direction. In this case we have available only the x -component of the slowness vector, which is represented by $p_1 = \xi + \Delta \xi$. If none of the perturbations $\Delta \eta$ and $\Delta \zeta$ is known we can obtain the equation for inversion by eliminating these perturbations from Equations 2.10 and 2.11. Eliminating firstly $\Delta \eta$ we obtain the set of equations:

$$\eta (\alpha^2 - \beta^2)^{-1} B_{K3} - \frac{1}{2} \alpha^{-3} B_{33} e_3^{(K)} = \eta g_i e_i^{(K)} - \alpha \Delta \xi (\eta e_1^{(K)} - \xi e_3^{(K)}) - \alpha \Delta \zeta X^{(K)}, K = 1, 2, \quad (2.18)$$

where

$$X^{(K)} = \eta e_2^{(K)} - \zeta e_3^{(K)}, \quad (2.19)$$

then we eliminate $\Delta \zeta$ from Equation 2.18 and rearrange it in such way that we find the following equation:

$$(\alpha^2 - \beta^2)^{-1} (B_{13} e_1^{(1)} + B_{23} e_1^{(2)}) + \frac{1}{2} \alpha^{-1} B_{33} \xi = g_i (e_i^{(1)} e_1^{(1)} + e_i^{(2)} e_1^{(2)}) - \alpha \Delta \xi. \quad (2.20)$$

2.2 DETERMINATION OF THE REFERENCE MEDIUM PARAMETERS

Inversion Equations 2.17 and 2.20 depend on isotropic reference parameters: P -wave velocity α , S -wave velocity β and wave normal vector of the P -wave n_i . The determination of α is made by the following relationship:

$$p_i = \alpha^{-1} g_i. \quad (2.21)$$

The symbols p_i and g_i corresponds to slowness component observed (z -component for vertical wellbore and x -component for horizontal wellbore) and polarization vector, respec-

tively. Thus, the velocity α can be obtained from least-squares inversion of Equation 2.21. The S -wave velocity β is determined by assuming that the reference medium is a Poisson solid, defined as:

$$\beta = \frac{\alpha}{\sqrt{3}}. \quad (2.22)$$

The wave normal vector n_i is considered parallel to the polarization vector observed, so $n \parallel g$. This approximation is valid for weakly anisotropic medium.

2.3 INVERSION SCHEME

WA parameters of the medium in the vicinity of borehole receivers can be estimated by inverting the appropriate equation for wellbore orientation, i.e., Equations 2.17 for data observed in vertical borehole or Equation 2.20 for data observed in horizontal borehole. For inversion procedure the suitable equation can be represented in matrix form:

$$\mathbf{G} \mathbf{m} = \mathbf{d}. \quad (2.23)$$

The symbol \mathbf{d} represents a vector which is related to the observations, this vector is given by right side of used equation (i.e, Equations 2.17 or 2.20) for each source–receiver pair and has dimension equal to the number of observations (N_{obs}). Symbol \mathbf{m} denotes the vector of model parameters, hence it consists of 15 WA parameters and has the form:

$$\mathbf{m} = [\epsilon_x, \epsilon_y, \epsilon_z, \delta_x, \delta_y, \delta_z, \chi_x, \chi_y, \chi_z, \epsilon_{15}, \epsilon_{16}, \epsilon_{24}, \epsilon_{26}, \epsilon_{34}, \epsilon_{35}]^T. \quad (2.24)$$

Finally, \mathbf{G} represents a linear operator, called sensitivity matrix, which depends on the parameters of reference medium and the design of VSP experiment. The matrix \mathbf{G} has dimension $N_{obs} \times 15$ and its elements are obtained from left side of used equation, i.e. taking the partial derivatives with respect to model parameters.

Equation 2.23 is solved by generalized inverse (Aster et al., 2011). Therefore, the solution can be written as

$$\mathbf{m}^{est} = \mathbf{G}^\dagger \mathbf{d}, \quad (2.25)$$

where \mathbf{m}^{est} is the vector of estimated parameters, which is a least squares solution, and \mathbf{G}^\dagger is the generalized inverse of \mathbf{G} . The singular value decomposition (SVD) is used to compute a generalized inverse. The SVD representation of \mathbf{G} is given by

$$\mathbf{G} = \mathbf{U} \mathbf{S} \mathbf{V}^T, \quad (2.26)$$

where \mathbf{U} and \mathbf{V} are orthonormal matrices of eigenvectors that span the data space and model parameters space, respectively, and the superscript T denotes transposition. \mathbf{S} is the diagonal matrix whose diagonal elements are the singular values $\lambda_1, \lambda_2, \dots, \lambda_{15}$. Thus,

the generalized inverse is expressed as

$$\mathbf{G}^\dagger = \mathbf{V} \mathbf{S}^{-1} \mathbf{U}^T, \quad (2.27)$$

and the solution as

$$\mathbf{m}^{\text{est}} = \mathbf{V} \mathbf{S}^{-1} \mathbf{U}^T \mathbf{d}. \quad (2.28)$$

3 EXPERIMENTAL DESIGN

In multiazimuth walkaway VSP surveys, as shown by Barreto et al. (2013), at least five radial profiles are necessary so that all 15 WA parameters can be independently retrieved. Additionally, we extend the analysis for other types of acquisition geometries. Thus, three distribution of sources on the surface are considered: along five radial profiles, randomly distributed and in spiral pattern. Moreover, they are also considered two wellbore configurations: vertical and horizontal borehole. In the numerical experiments conducted in this work, the observed data (polarization and slowness components of qP -wave) are generated using the program package ANRAY (Gajewski and Pšenčík, 1990). In the following sections it is described the survey geometries and the features of synthetic model. Furthermore, it discussed about the sensitivity analysis with respect to survey design and the procedures employed in this analysis.

3.1 MODEL AND CONFIGURATION OF EXPERIMENTS

The model consists of two layers confined in a box with following dimensions: length 10 km, width 10 km and height 7 km. The origin of Cartesian coordinate system (x, y, z) is situated in the center of the model. The interface between layers is located at a depth of 5 km and has geometry flat horizontal.

The first layer is heterogeneous anisotropic with anisotropy degree about 8%. The distribution of elastic parameters (21 density-normalized elastic parameters) is given by linear interpolation between the values of parameters specified at the top ($z = 0$ km) and at the bottom ($z = 5$ km) of the layer. The elastic parameters at top surface corresponds to VTI (transversely isotropy with a vertical symmetry axis) medium with symmetry axis rotated by 80° around the y -axis and then 25° around the z -axis. The non-rotated matrix of the density-normalized elastic moduli in $(km/s)^2$ of initial VTI medium is

$$A_{ij} = \begin{bmatrix} 15.71 & 5.05 & 4.46 & 0.00 & 0.00 & 0.00 \\ & 15.71 & 4.46 & 0.00 & 0.00 & 0.00 \\ & & 13.39 & 0.00 & 0.00 & 0.00 \\ & & & 4.98 & 0.00 & 0.00 \\ & & & & 4.98 & 0.00 \\ & & & & & 5.33 \end{bmatrix}. \quad (3.1)$$

The elastic parameters at bottom surface corresponds to VTI medium with symmetry axis rotated by 90° around the y -axis. The non-rotated matrix of the density-normalized elastic moduli in $(km/s)^2$ of VTI medium is

$$A_{ij} = \begin{bmatrix} 35.35 & 11.36 & 10.04 & 0.00 & 0.00 & 0.00 \\ & 35.34 & 10.04 & 0.00 & 0.00 & 0.00 \\ & & 30.13 & 0.00 & 0.00 & 0.00 \\ & & & 11.21 & 0.00 & 0.00 \\ & & & & 11.21 & 0.00 \\ & & & & & 11.99 \end{bmatrix}. \quad (3.2)$$

The second layer is a homogeneous isotropic medium, which is characterized by density-normalized P - and S -wave velocities of 4.77 km/s and 2.76 km/s, respectively.

In this study was simulated VSP surveys with receivers located in a vertical and horizontal borehole (see Figure 3.1). In the first situation the borehole is situated in the center of the model, hence the receivers array is in the direction of the z -axis(see Figure 3.1a). In the horizontal wellbore experiment the receivers array is located at a depth of 0.5 km and parallel to positive direction of the x -axis(see Figure 3.1b).

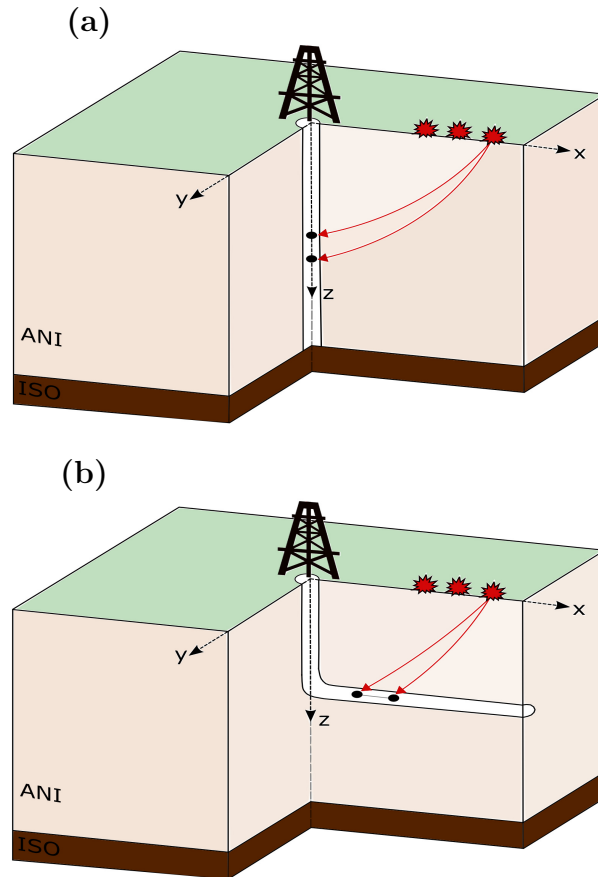


Figure 3.1: Schematic illustration of models with receiver in vertical and horizontal borehole. The first layer (ANI) is heterogeneous anisotropic and the second one (ISO) is homogeneous isotropic. (a) Vertical borehole with receivers in the direction of the z -axis. (b) Horizontal borehole with receivers parallel to the x -axis direction.

Three types of distribution of sources on the surface are considered in the tests (see Figure 3.2). In the first one, the sources are distributed along five radial profiles with angular steps of 72° . The middle of each profile intersects the center of the model and the sources are regularly spaced by 0.1 km along each profile, starting from the center of the model. The second one consists of randomly distribution of sources over the surface of the model. Finally, in the third distribution type is used a spiral pattern with dual sources array. In the two spirals, the distance of first source point from the center of the model is 0.1 km.

In the VSP experiments with vertical borehole configuration, we used 90 sources for each survey layouts. The observed data set (computed by ANRAY package) comprises the three components of polarization and vertical component of slowness of direct and reflected qP -wave for each source–receiver pair. The number of sources, the orientation of five profiles are based on experimental setup used in the study of Barreto et al. (2013).

In the experiments with horizontal borehole configuration, we used 180 sources for the three type of source distribution. The observed data set (computed by ANRAY package) comprises the three components of polarization and x -component of slowness of direct qP -wave for each source–receiver pair. The larger number of sources is due to the use of only direct qP -wave measurements.

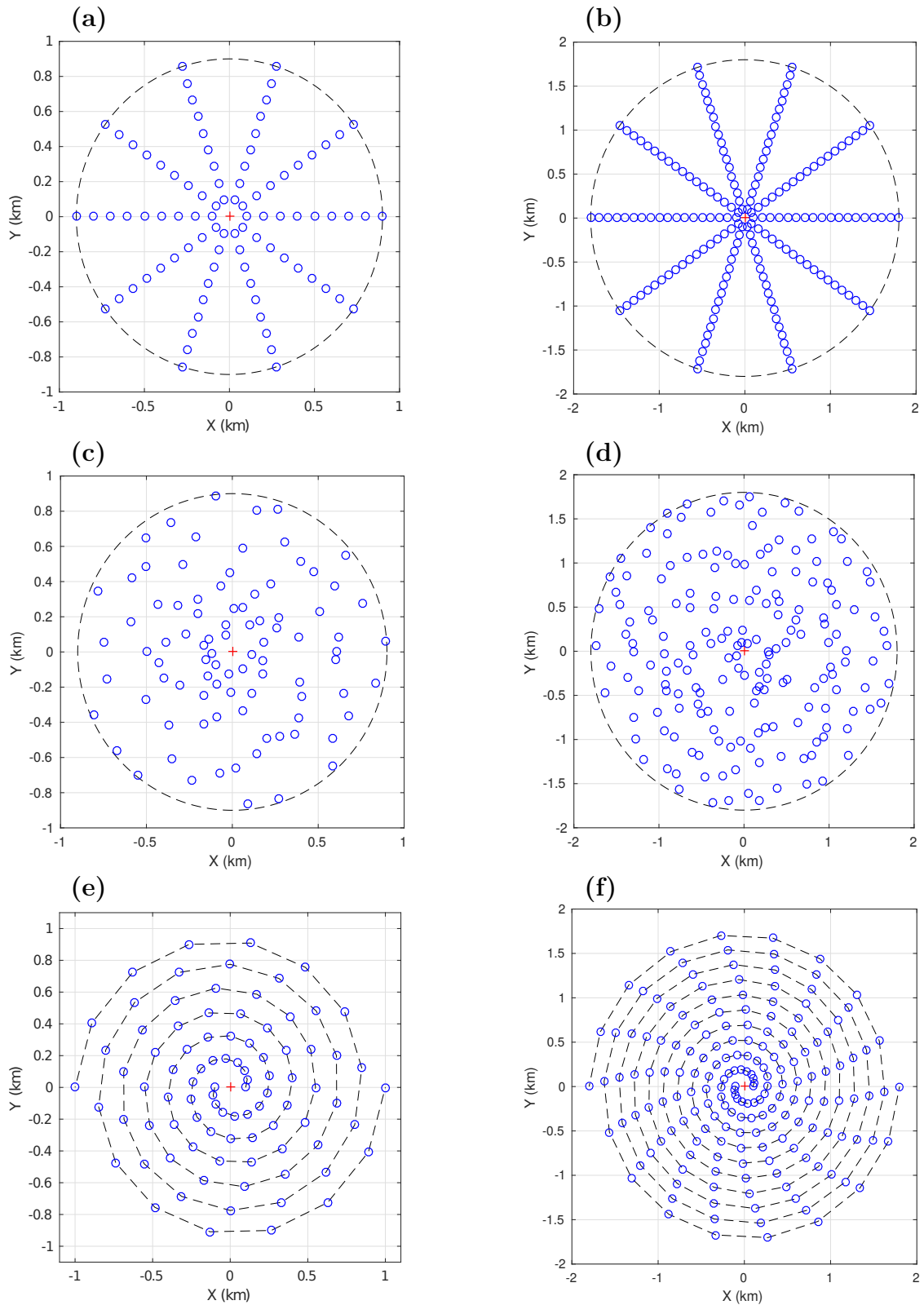


Figure 3.2: Plan view of the acquisition geometries used in the numerical tests. Three types of source distribution are considered: five radial profiles (with angular steps of 72°), randomly and spiral pattern. 90 sources are used in VSP experiments with vertical borehole configuration (Fig.3.2a, Fig.3.2c and Fig.3.2e). For VSP experiments with horizontal borehole configuration, 180 sources are employed (Fig.3.2b, Fig.3.2d and Fig.3.2f).

3.2 SENSITIVITY STUDY

The ability to retrieve the WA parameters depends heavily on the design of VSP surveys. A sensitivity analysis makes it possible to determine how to optimize seismic measurements in order to enable the recovery of parameters with better resolution. Here, the sensitivity analysis of estimation with respect to acquisition geometry was carried out in two stages. The first one is based on the model resolution matrix. The second stage consists of numerical computation of model covariance.

The first stage of the analysis is conducted for only one receiver inside each wellbore. For the vertical borehole configuration is considered the receiver at a depth of 0.5 km and for the horizontal one is considered the receiver at a depth of 0.5 km and 0.4 km away from z -axis.

The model resolution matrix determines whether model parameters can be independently predicted or calculated, so it is a useful tool in experimental design (Menke, 2012). The resolution matrix \mathbf{R} can be calculated from singular value decomposition (SVD) of sensitivity matrix \mathbf{G} (see Equation 2.26) in the following way:

$$\mathbf{R} = \mathbf{V}_r \mathbf{V}_r^T. \quad (3.3)$$

In Equation 3.3, \mathbf{V}_r is a submatrix of \mathbf{V} , which has dimension 15 x 15 (i.e., the number of parameters). Hence, the matrix \mathbf{V}_r consists of the first r columns of \mathbf{V} , the columns of \mathbf{V}_r are the vectors $\mathbf{v}^{(1)}$ to $\mathbf{v}^{(r)}$, which are eigenvectors associated with the acceptable singular values, i.e., those greater than a specified cutoff value. This value is chosen by prescribing an acceptable condition number for matrix \mathbf{G} . The condition number is defined as the ratio of the largest to smallest singular value.

Figure 3.3 shows the singular values computed for the three acquisition geometries in VSP experiment with vertical borehole. Comparing the results, it can be seen that the behavior of the singular values does not differ much. The condition number in the three cases are smaller than 100. For this inverse problem, the selected cutoff value was 0.01. It observed that for the three geometries none of singular values are smaller than 0.01, consequently all columns of \mathbf{V} are considered in the computation of matrix resolution.

The analysis of the singular value shows that the sensitivity matrix \mathbf{G} for the three distributions of sources is of full rank, since all the singular values are considered nonzero. Therefore, the computation of the model resolution matrices yields identity matrices (see Figure 3.4), then each of 15 WA parameter is uniquely determined for the three distributions.

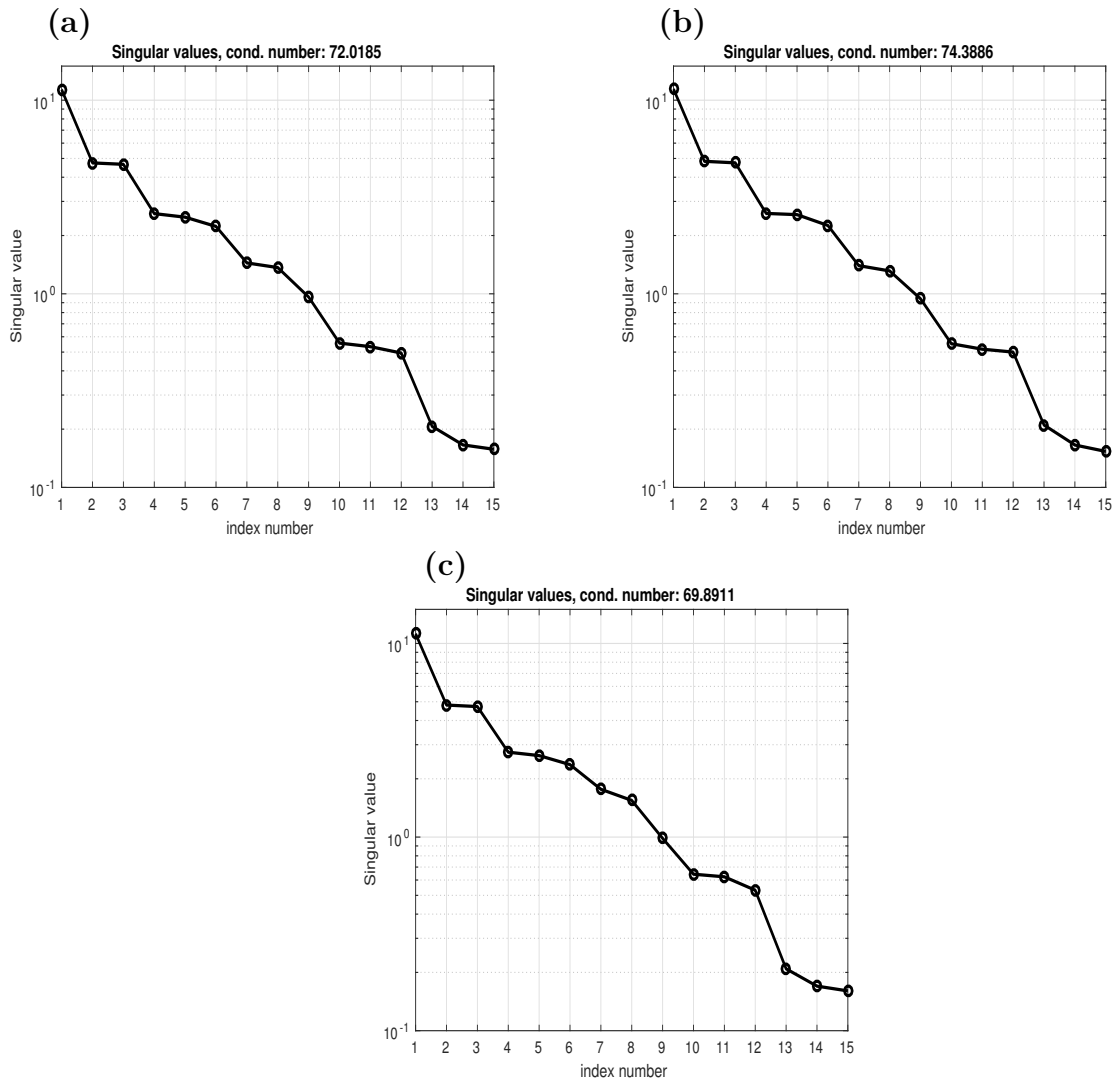


Figure 3.3: Singular values for the three acquisition geometries (see Figure 3.2) of VSP experiments with vertical borehole. The vertical axes are in logarithmic scale. (a) Result for sources along five profiles. (b) Result for sources randomly distributed. (c) Result for sources in spiral pattern.

Figure 3.5 shows the singular values computed for VSP experiments with horizontal borehole. Here, similarly to results for vertical borehole configuration, the condition numbers obtained for the three geometries are also smaller than 100. The selected cutoff value was 0.01 as well. Given that all singular values in the three cases are smaller than 0.01, the sensitivity matrix \mathbf{G} is of full rank and the model resolution matrix is equal a identity matrix, which means that each of 15 WA parameter is uniquely determined.

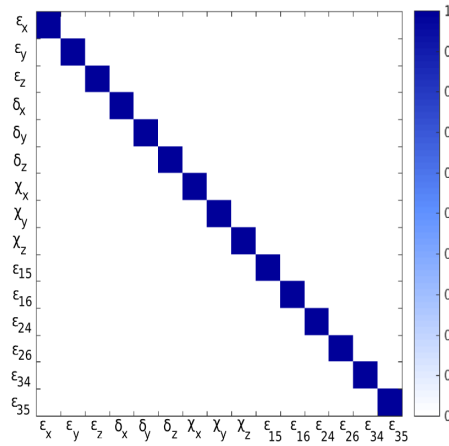


Figure 3.4: Model resolution matrix for the three acquisition geometries of VSP experiments with vertical borehole is equal to identity matrix, which means that all 15 parameters can be uniquely determined.

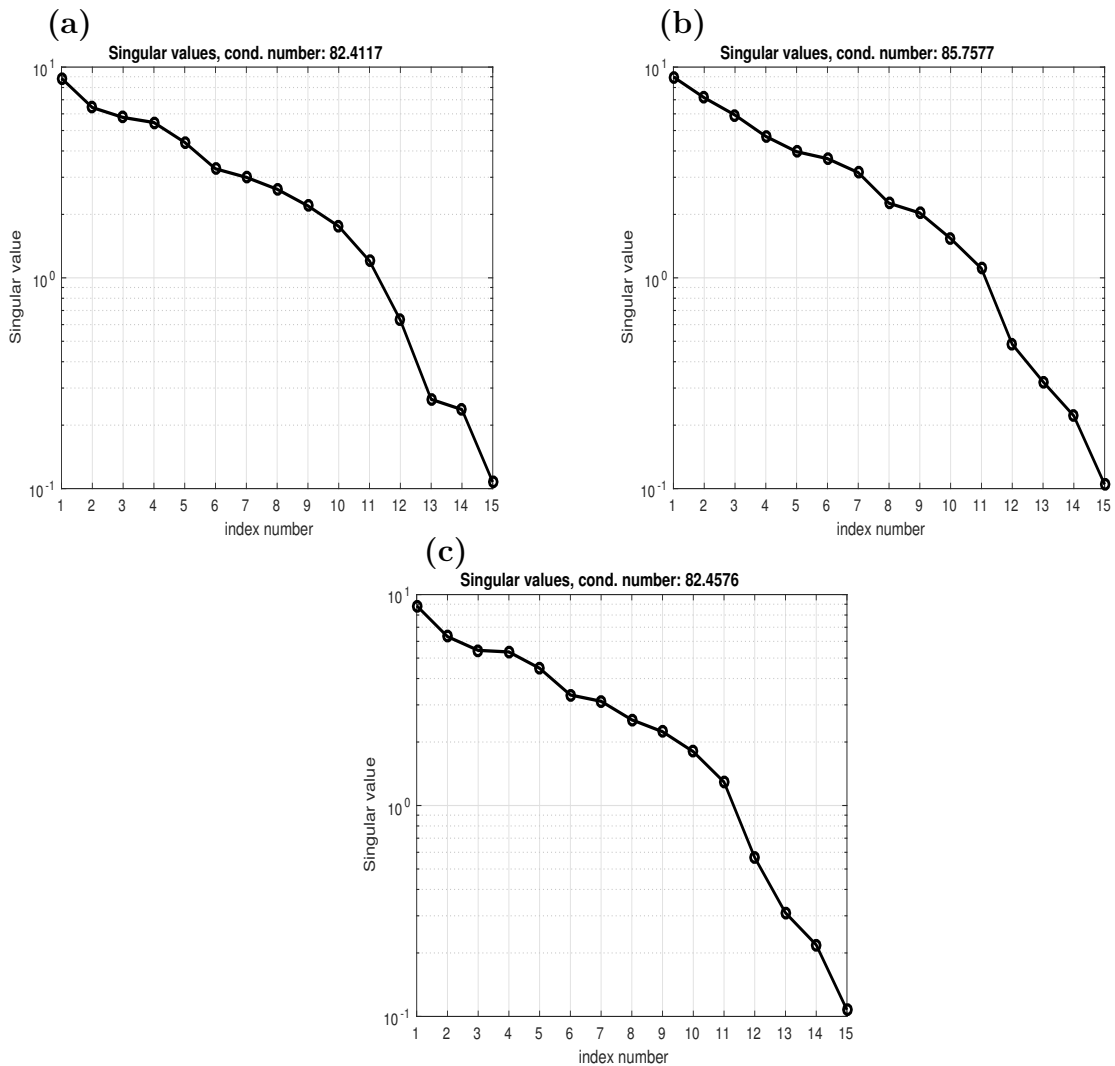


Figure 3.5: Singular values for the three acquisition geometries (see Figure 3.2) of VSP experiments with horizontal borehole. The vertical axes are in logarithmic scale. (a) Result for sources along five profiles. (b) Result for sources randomly distributed. (c) Result for sources in spiral pattern.

It is noteworthy that the above analysis of resolution is a means to assessing which of sought parameters can be uniquely estimated using the acquisition geometries studied. Nonetheless, the resolution of estimates is affected by noise in data, hence for the inversion results to be meaningful it is necessary to investigate how errors in the data projects errors in the estimated model. For this purpose, the model covariance matrix is computed.

Covariance is a measure of the strength to which two or more sets of parameters are correlated. The model covariance matrix characterizes the degree of error amplification that resulting from mapping the data into the model, hence it is a useful tool to estimate the reliability of the solution (Menke, 2012). In this sensitivity analysis, that tool is also used to provide information of how the acquisition geometry influences the model errors. The model covariance is computed using the parameters estimated from a set of 500 inversion trials, in which data contaminated by different noise sequences are inverted. Therefore, the numerical computation of this matrix is given by

$$\mathbf{C}_{ij} = \frac{1}{N} \sum_{k=1}^N (\mathbf{m}_i^{\text{est}} - \bar{\mathbf{m}}_i) (\mathbf{m}_j^{\text{est}} - \bar{\mathbf{m}}_j), \quad (3.4)$$

where \mathbf{C}_{ij} denotes the elements of covariance matrix, with $i, j = 1, 2, \dots, 15$. N stands for the number of different solutions \mathbf{m}^{est} obtained from inversion trials. Finally, the symbol $\bar{\mathbf{m}}$ corresponds to the vector of mean (expected) solution, which is obtained from the average of the N solutions \mathbf{m}^{est} . Computed covariance matrices are presented together with inversion results in the next chapter.

4 INVERSION TESTS

In the following, the inversion equations for qP -wave data recorded in vertical and horizontal borehole are tested. The inversion scheme is applied for synthetic data contaminated with random Gaussian noise. For direct qP -wave, the added noise has standard deviations of 1° for polarization vector and 5% for slowness data (z -component for vertical borehole configuration and x -component for horizontal configuration). For reflected wave, the noise contamination is twice the amount added to direct wave, situation that occurs in real data.

Tests are performed for data generated by the three types of source distribution (see Figure 3.2) with each wellbore configuration. For each dataset, the inversion is carried out 500 times for different realizations of noise and the model covariance matrix is computed from results of 500 simulations using Equation 3.4. The diagonal entries of the model covariance matrix are the variances of estimated parameters and the off-diagonal elements describe the correlation between pairs of parameters, that is, how two parameters change together. Since the noise in the data will cause errors in the model parameter estimates, the covariance values of the matrix characterize the degree of error amplification that occurs. Thus, the computed model covariance matrices are used to evaluate the uncertainty in the estimated model parameter.

The quality of WA parameters recovered from inversion is analyzed by computation of the first-order approximation of the phase velocity (Pšenčík and Gajewski, 1998) and comparing stereographic projections of phase velocity obtained with exact and inverted parameters. The first-order approximation of phase velocity is calculated by the following formula:

$$c(n_i, m_j) = \sqrt{\alpha^2 + B_{33}}. \quad (4.1)$$

In Equation 4.1, the element of the weak anisotropy matrix B_{33} is given by Equation 2.14 and α stands for the P -wave velocity of the reference isotropic medium. This expression for phase velocity $c(n_i, m_j)$ depends on the wave normal vector n_i and the model parameters vector m_j , which consists of 15 WA parameters (see Equation 2.24).

For presentation of inversion results, four types of stereographic projection maps are shown: (a) the phase velocity calculated from the exact WA parameters; (b) the phase velocity calculated from the expected WA parameters from 500 inversion trials; (c) the relative error expressed as a percent between (b) and (a); and (d) the percentage variation of the phase velocity. The latter map is used for stability analysis of the estimates.

4.1 INVERSION RESULTS FOR VERTICAL BOREHOLE

For datasets measured within the vertical borehole, the inversion is performed at two receivers using Equation 2.17. The receiver 1 and receiver 2 are located at depth of 0.1

and 0.5 km, respectively.

Before inversion procedure it is necessary to determine the velocities of the reference medium. Figure 4.1 shows P - and S -wave velocities obtained from least-squares fitting of polarization and slowness components in the wellbore direction (see relationship in Equation 2.21) to the receiver 1. The fitting procedure is carried out to datasets generated by the three sources distributions (i.e, along five radial profiles, randomly distributed and in spiral pattern). For each dataset, the results corresponds to the mean of estimates for 500 realizations of random noise. Note that the values obtained for the three experiments are very close, therefore the velocity determination of the reference isotropic medium has little influence of the acquisition geometry.

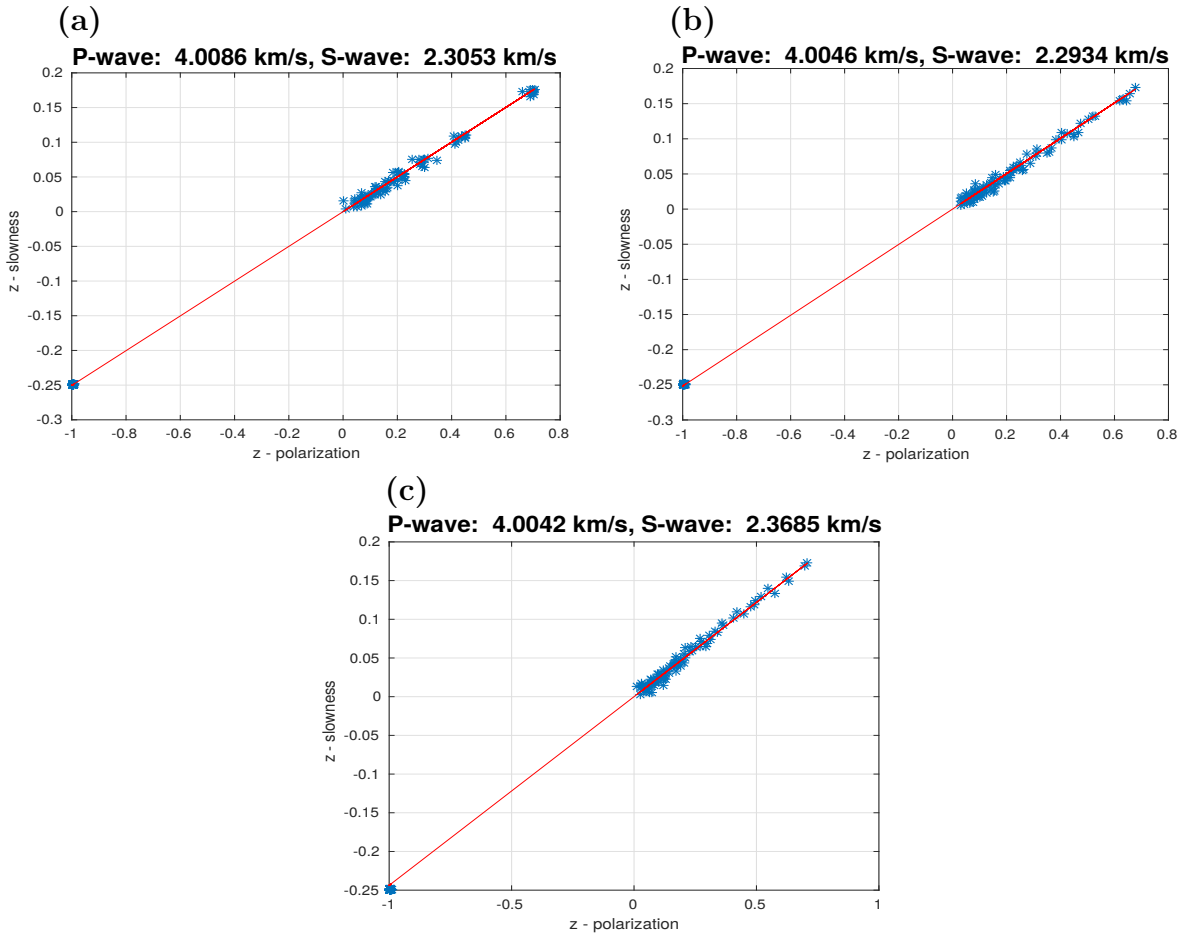


Figure 4.1: Estimated velocities of the reference isotropic medium to the receiver 1 of the vertical borehole. The estimation is based on Eq. 2.21 and uses the components of the slowness and polarization along z -axis of the direct and reflected wave. Results for the three acquisition geometries: (a) sources along 5 profiles, (b) random sources, (c) spiral sources pattern.

Figure 4.2 shows the covariance matrices calculated for the three sources geometries to the receiver 1. It is possible to note that the 15 WA parameters can be divided into two groups regarding the degree of uncertainty. There is greater uncertainty in the determination of parameters ϵ_x , ϵ_y , δ_x , δ_y , δ_z , χ_z , ϵ_{16} and ϵ_{26} . For the other parameters

the uncertainty is much smaller. Comparing the three matrices, it is observed that the diagonal values, which is the variance, corresponding to the first group of parameters are greater for randomly and spiral distribution. Furthermore, the correlation between these WA parameters, given by off-diagonal values, is stronger for spiral geometry and then for randomly distribution. For second group of parameters $\epsilon_z, \chi_x, \chi_y, \epsilon_{15}, \epsilon_{24}, \epsilon_{34}$ and ϵ_{35} the values of variance and correlation are similar for the three geometries.

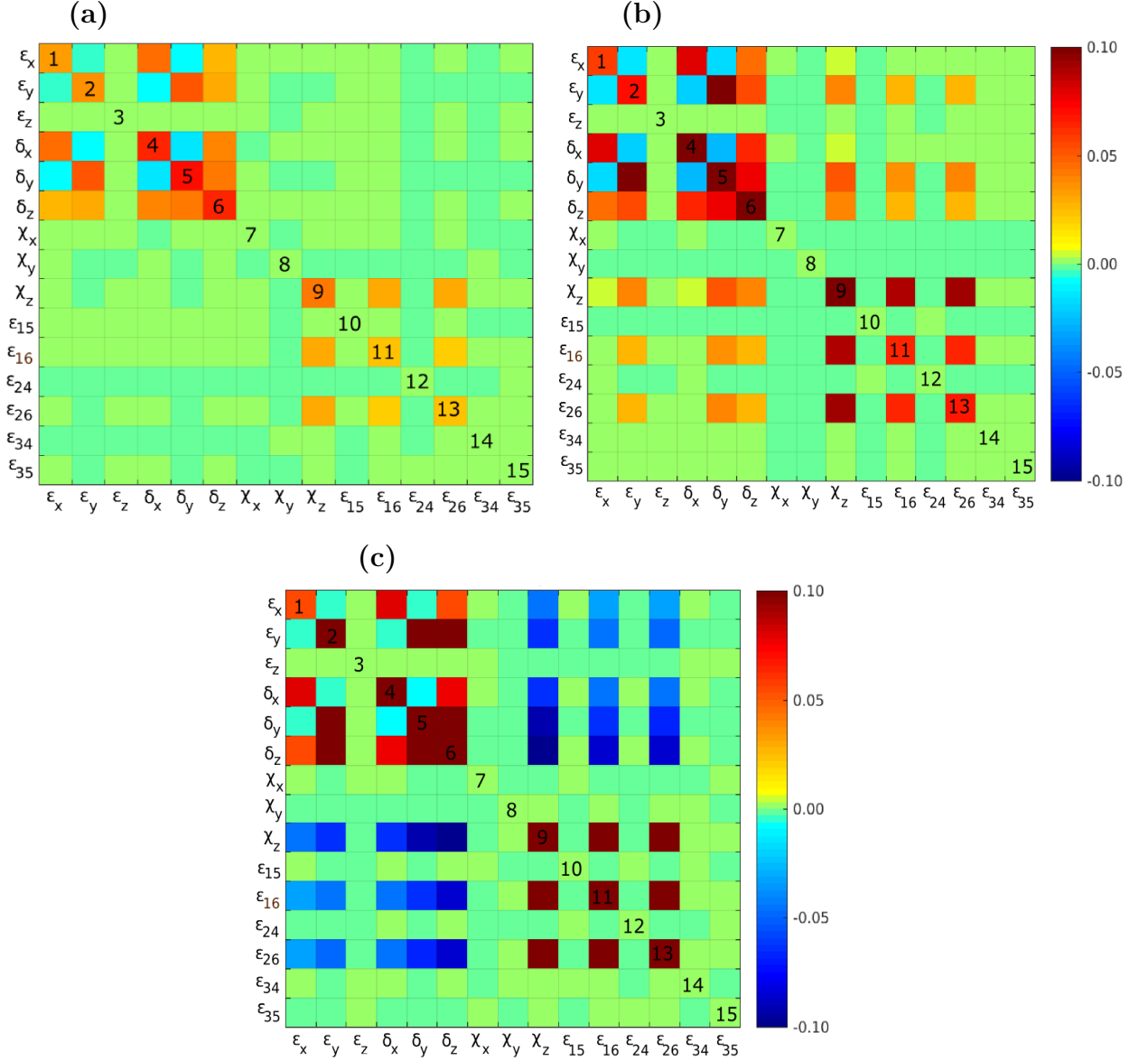


Figure 4.2: Model covariance matrices computed for experiments using the three acquisition geometries to the receiver 1 of the vertical borehole. (a) For sources along 5 profiles. (b) For random sources. (c) For spiral sources pattern.

Figure 4.3 shows the following stereographic maps to the receiver 1: phase velocity computed using exact WA parameters (Figure 4.3a), using estimated parameters from data generated by sources along five profiles (Figure 4.3b), randomly distributed (Figure 4.3c)

and in spiral pattern (Figure 4.3d). It also shows stereographic projection of percentage error between estimated maps and the exact one (Figure 4.3e, Figure 4.3f and Figure 4.3g). Comparing the results for the three source distributions, it can be observed that in all three cases the percentage error does not exceed 2.5%, and among the three experiments, the spiral geometry produces the largest error. Given that the model used in the tests exhibits anisotropy strength about 8%, we consider that the phase velocities are well estimated for error below 4%.

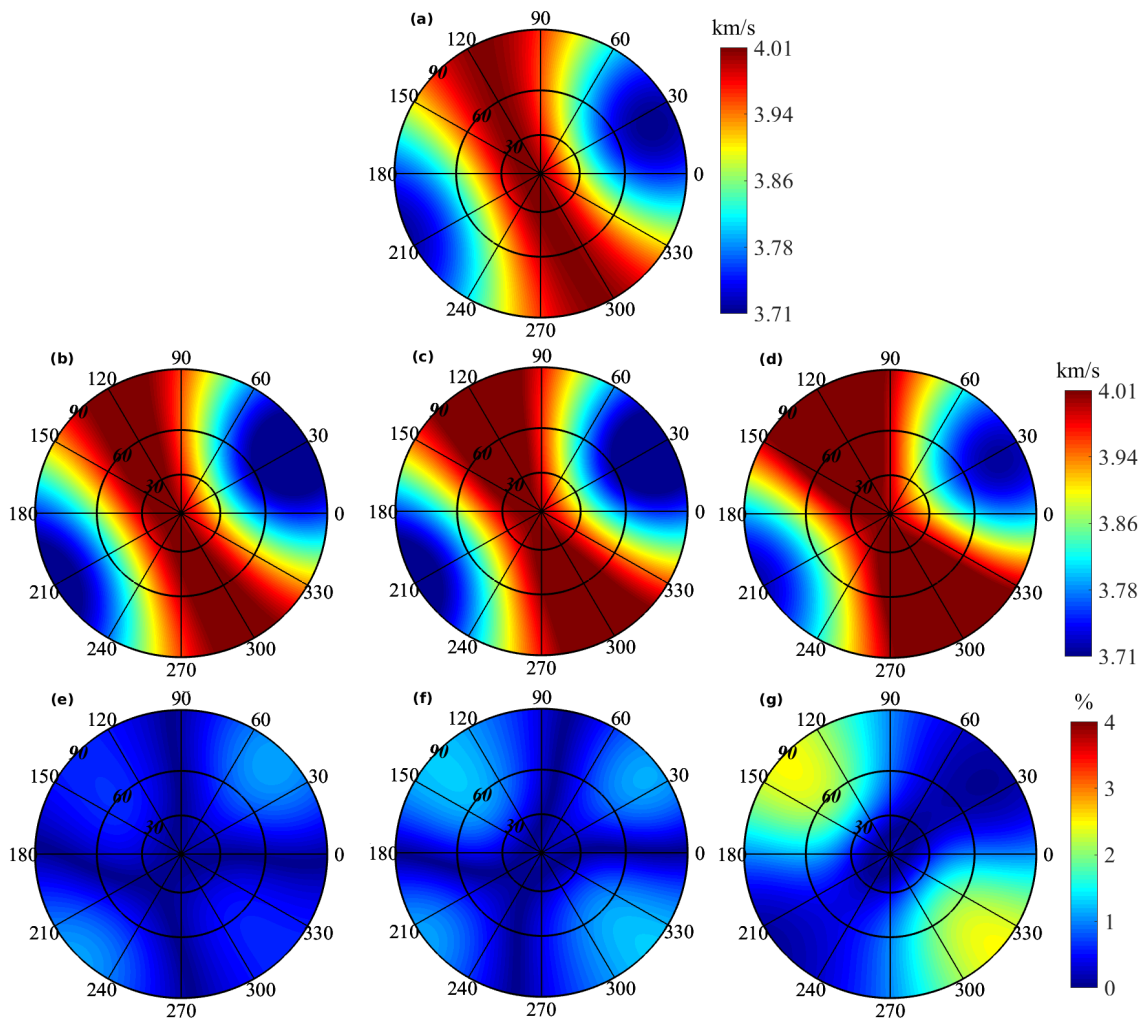


Figure 4.3: Stereographic maps to the receiver 1 of the vertical borehole. (a) Phase velocity computed using exact WA parameters. (b) Phase velocity computed using estimated WA parameter for experiment with sources distributed along five profiles. (c) Phase velocity computed using estimated WA parameter for experiment with sources distributed randomly. (d) Phase velocity computed using estimated WA parameter for experiment with sources distributed in spiral pattern. (e) Percentage error between (a) and (b). (f) Percentage error between (a) and (c). (g) Percentage error between (a) and (d).

Figure 4.4 shows percentage variation maps of phase velocity. It is calculated from phase velocity computed using the parameters estimated in each of the 500 simulations. The results for sources distributed along five profiles, randomly and in spiral pattern are

shown in Figure 4.4a, Figure 4.4b and Figure 4.4c, respectively. According to these figures, it is observed that the phase velocity suffers less variation around the vertical axis. As the polar angle increases the velocity variation also increases. The best estimates are obtained within the region delimited by a 30° cone around the wellbore direction. Comparing the results for the three sources geometries, we note that the variation is greater for the spiral geometry and then for the random distribution, for which the variation exceeds 10% in some regions within 30° cone.

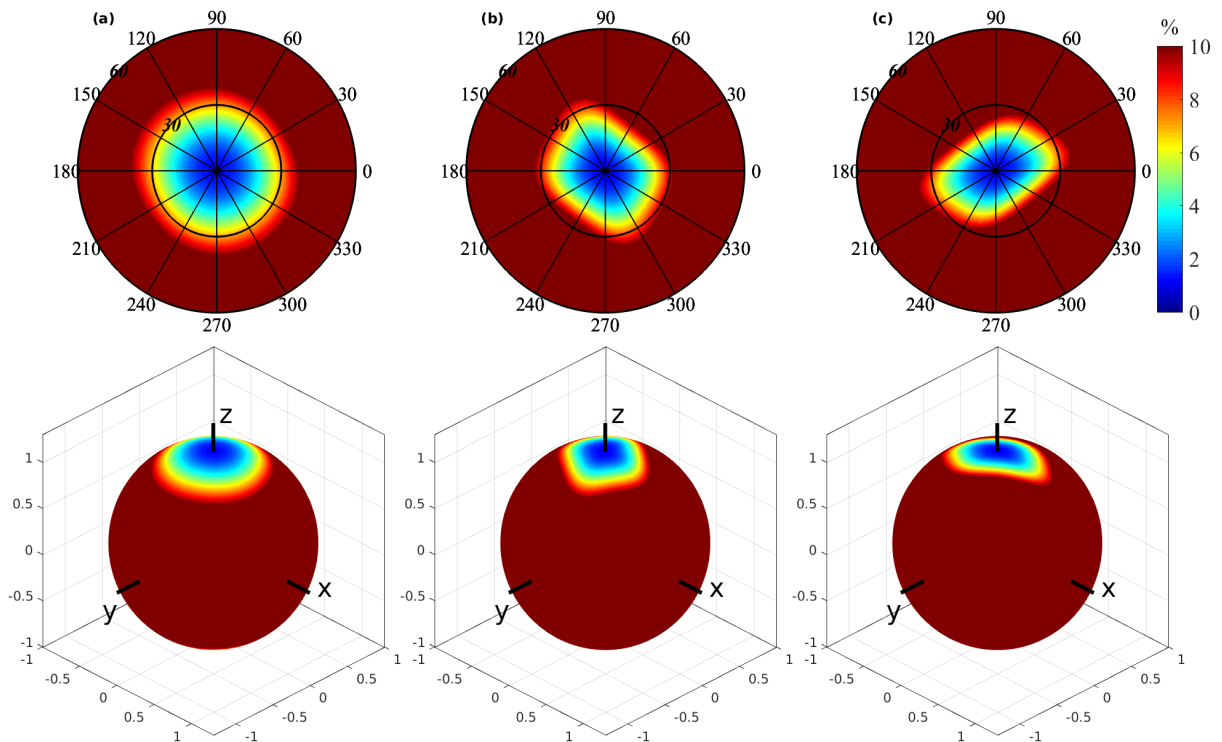


Figure 4.4: Percentage variation maps (stereographic projections and its corresponding spherical surfaces) of phase velocity to the receiver 1 of the vertical borehole. (a) Results for sources along 5 profiles. (b) Results for sources distributed randomly. (c) Results for sources distributed in spiral pattern.

The results for the receiver 2 are shown in the following. Figure 4.5 shows the estimated velocities of the reference medium in the vicinity of this receiver. Similarly to the receiver 1, the values obtained for the three geometries are very close, which indicate that the source distribution has low influence in the determination of P - and S -wave velocities of reference medium.

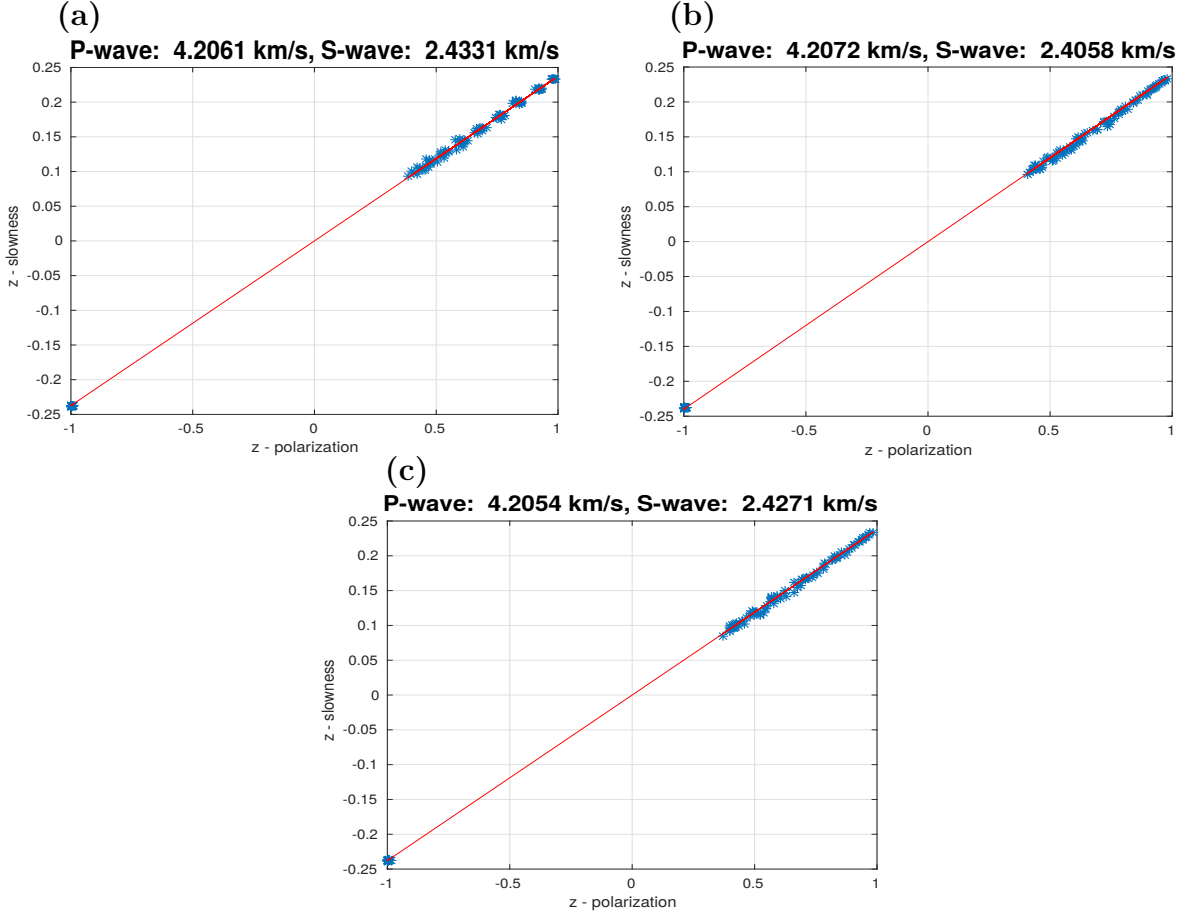


Figure 4.5: Estimated velocities of the reference isotropic medium to the receiver 2 of the vertical borehole. The estimation is based on Eq. 2.21 and uses the components of the slowness and polarization along z-axis of the direct and reflected wave. Results for the three acquisition geometries: (a) sources along 5 profiles, (b) random sources, (c) spiral sources pattern.

Figure 4.6 shows the computed covariance matrices for the three acquisition geometries. Here, in contrast to the receiver 1, the general patterns (i.e., diagonal and off-diagonal values) of three matrices are similar. Thus, for this receiver the difference between the illuminations provided by the three source distributions has no significant effects in the error amplification and uncertainty in the estimates. In the case of the receiver 1, it is believed that the random and spiral distributions provided worst illumination of the medium at shallow depth which yields higher error in the corresponding matrices (see Figure 4.2). Besides, we note that there is greater uncertainty in the determination of parameters ϵ_x , ϵ_y , δ_x , δ_y , δ_z , χ_z , ϵ_{16} , while for the remaining parameters ϵ_z , χ_x , χ_y , ϵ_{15} , ϵ_{24} , ϵ_{34} and ϵ_{35} the uncertainty is lower. That is the same behavior observed to the receiver 1.

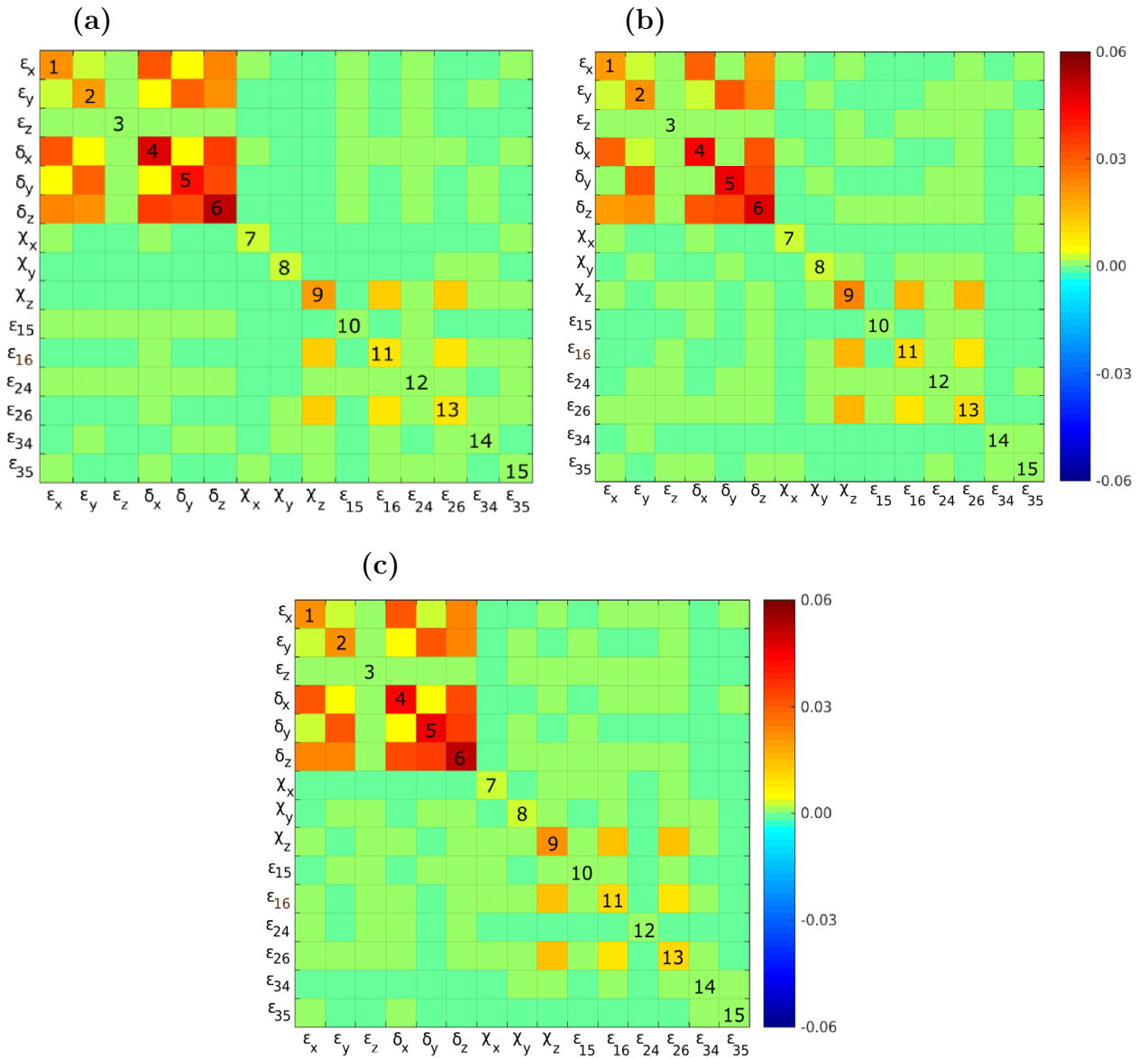


Figure 4.6: Model covariance matrices computed for experiments using the three acquisition geometries to the receiver 2 of the vertical borehole. (a) For sources along 5 profiles. (b) For random sources. (c) For spiral sources pattern.

Figure 4.7 shows the stereographic maps of phase velocity computed using exact WA parameters (Figure 4.7a), using estimated parameters from data generated by sources along five profiles (Figure 4.7b), randomly distributed (Figure 4.7c) and in spiral pattern (Figure 4.7d), and the stereographic projection of percentage error (Figure 4.7e, Figure 4.7f and Figure 4.7g) between estimated maps and the exact one. It can be seen that estimated phase velocities and percentage error are similar for the three source distributions. Note that error does not exceed 2.5%.

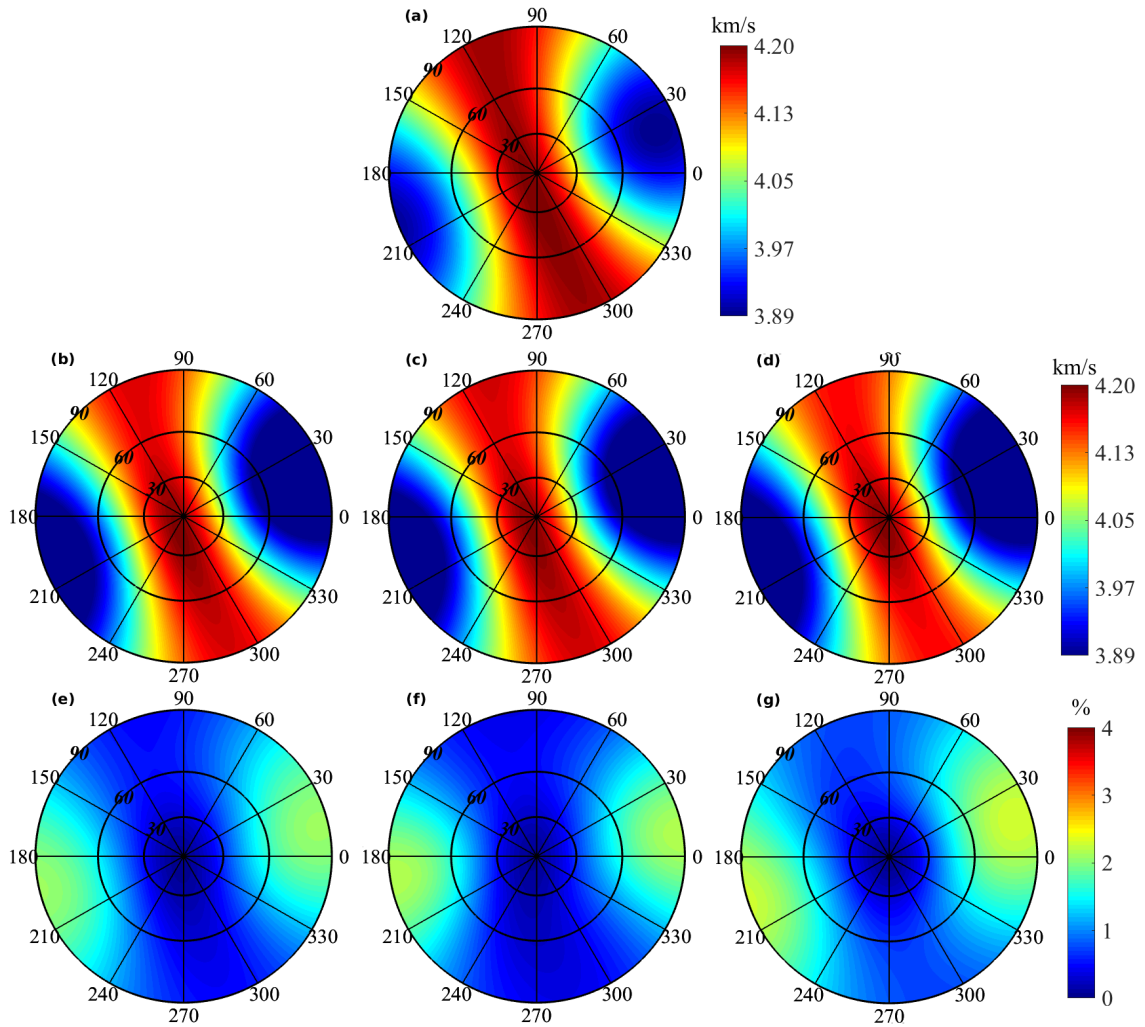


Figure 4.7: Stereographic maps to the receiver 2 of the vertical borehole. (a) Phase velocity computed using exact WA parameters. (b) Phase velocity computed using estimated WA parameter for experiment with sources distributed along five profiles. (c) Phase velocity computed using estimated WA parameter for experiment with sources distributed randomly. (d) Phase velocity computed using estimated WA parameter for experiment with sources distributed in spiral pattern. (e) Percentage error between (a) and (b). (f) Percentage error between (a) and (c). (g) Percentage error between (a) and (d).

Figure 4.8 shows percentage variation maps of phase velocity. It is obtained from phase velocity computed in each of the 500 inversions trials. The results for sources distributed along five profiles, randomly and in spiral pattern are shown in Figure 4.8a, Figure 4.8b and Figure 4.8c, respectively. Similarly to the receiver 1, the phase velocity suffers less variation around the vertical axis and best estimates are found within the region delimited by a 30° cone. Comparing the results obtained for the three sources geometries, it is observed that the variation is similar for the three experiments.

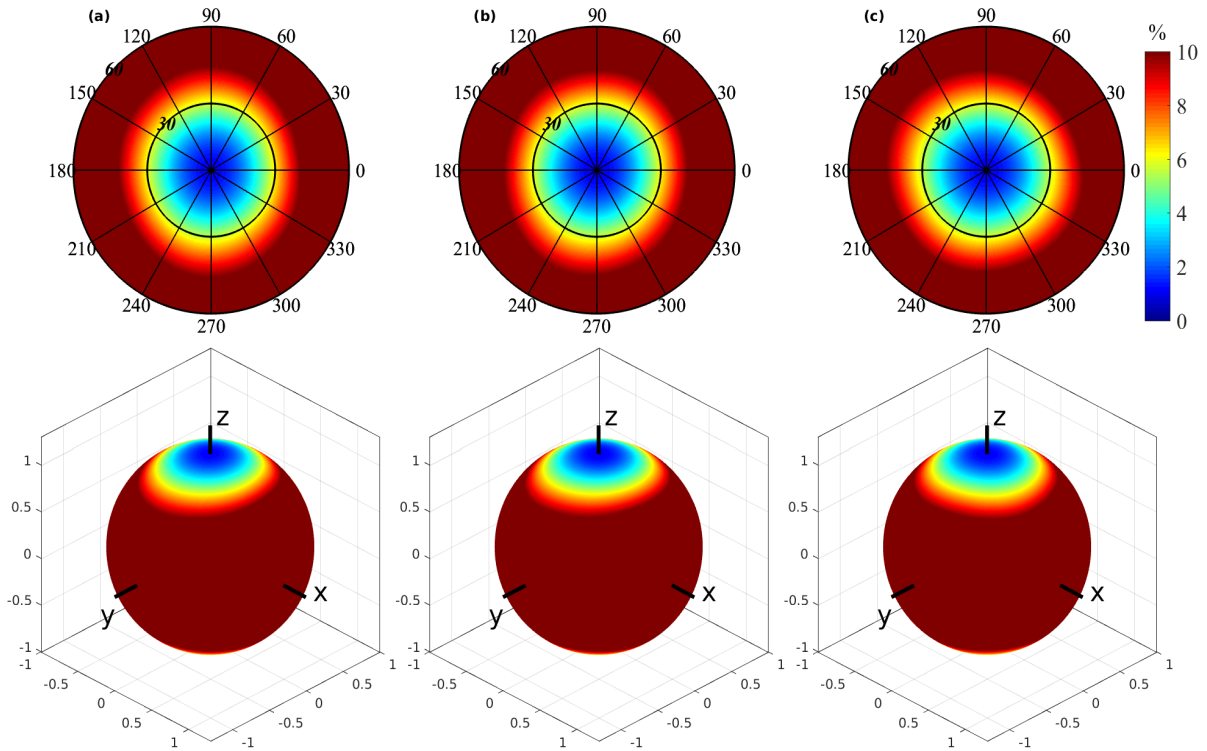


Figure 4.8: Percentage variation maps (stereographic projections and its corresponding spherical surfaces) of phase velocity to the receiver 2 of the vertical borehole. (a) Results for sources along 5 profiles. (b) Results for sources distributed randomly. (c) Results for sources distributed in spiral pattern.

4.2 INVERSION RESULTS FOR HORIZONTAL BOREHOLE

For datasets measured in the horizontal borehole, the inversion is carried out using Equation 2.20. In the tests is considered one receiver located at 0.5 km depth, in the same direction of the positive x -axis and 0.4 km away from z -axis.

Figure 4.9 shows the P - and S -wave velocities of the reference isotropic medium obtained from least-squares fitting of polarization and slowness components in the wellbore direction (see relationship in Equation 2.21). The results corresponds to the mean of estimates for 500 realizations of random noise. The values obtained from datasets generated by the three types of sources distribution (Figure 4.9a, Figure 4.9b and Figure 4.9c) are very close. Thus, as for the vertical borehole configuration, the velocities determination of the reference isotropic medium has little influence of the acquisition geometry.

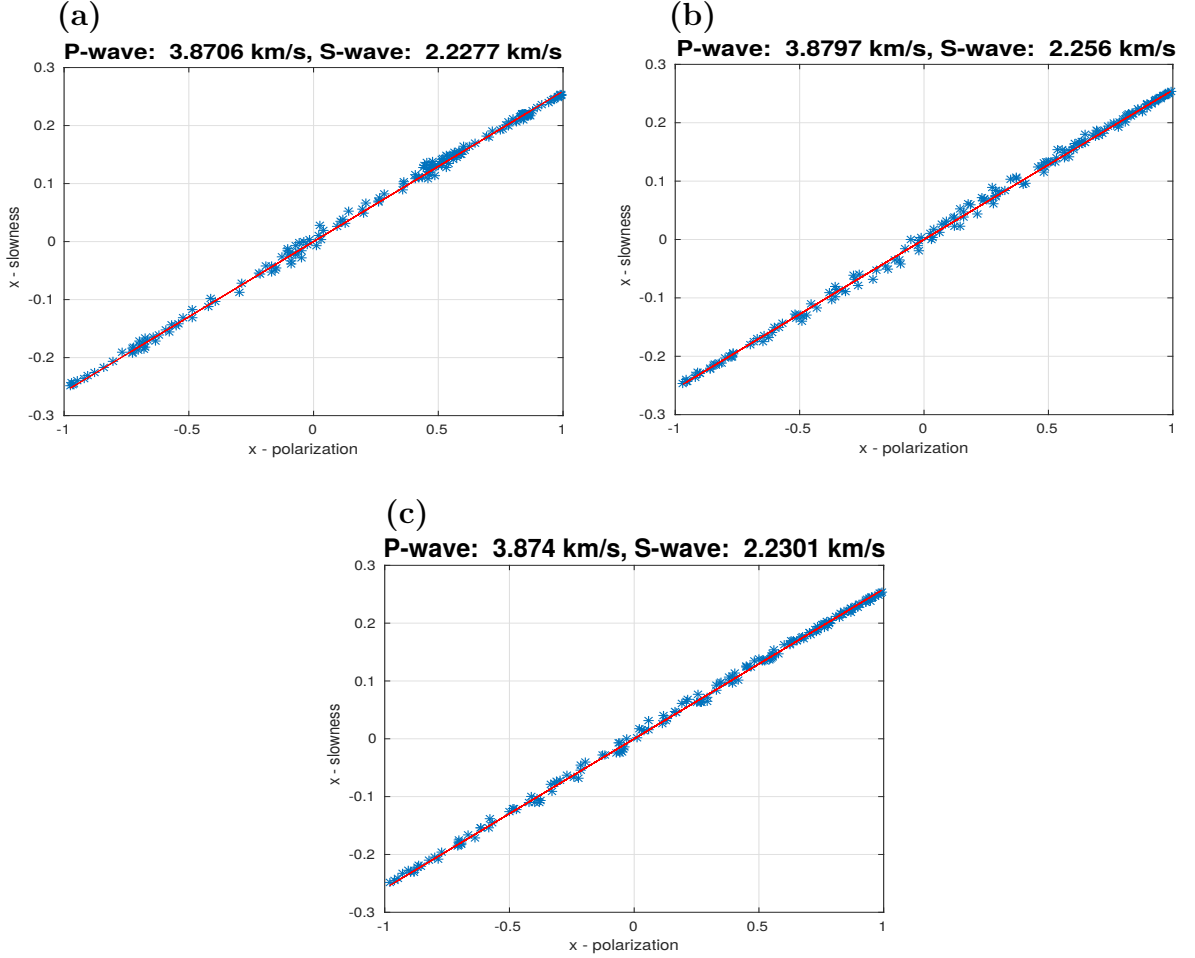


Figure 4.9: Estimated velocities of the reference isotropic medium to the receiver in the horizontal borehole. The estimation is based on Eq. 2.21 and uses the components of the slowness and polarization along x-axis of the direct wave. Results for the three acquisition geometries: (a) sources along 5 profiles, (b) random sources, (c) spiral sources pattern.

The covariance matrices calculated for experiments with the three sources geometries are shown in Figure 4.10. We note that general patterns in the three covariance matrices are similar. Based on values of variance (diagonal elements) and correlation between pair of parameters (off-diagonal elements), we note that there is higher uncertainty in the determination of parameters ϵ_y , ϵ_z , δ_x , δ_y , δ_z , moderate to χ_y , ϵ_{24} , ϵ_{34} , and lower uncertainty in the determination of parameters ϵ_x , χ_y , χ_z , ϵ_{15} , ϵ_{16} , ϵ_{26} and ϵ_{35} .

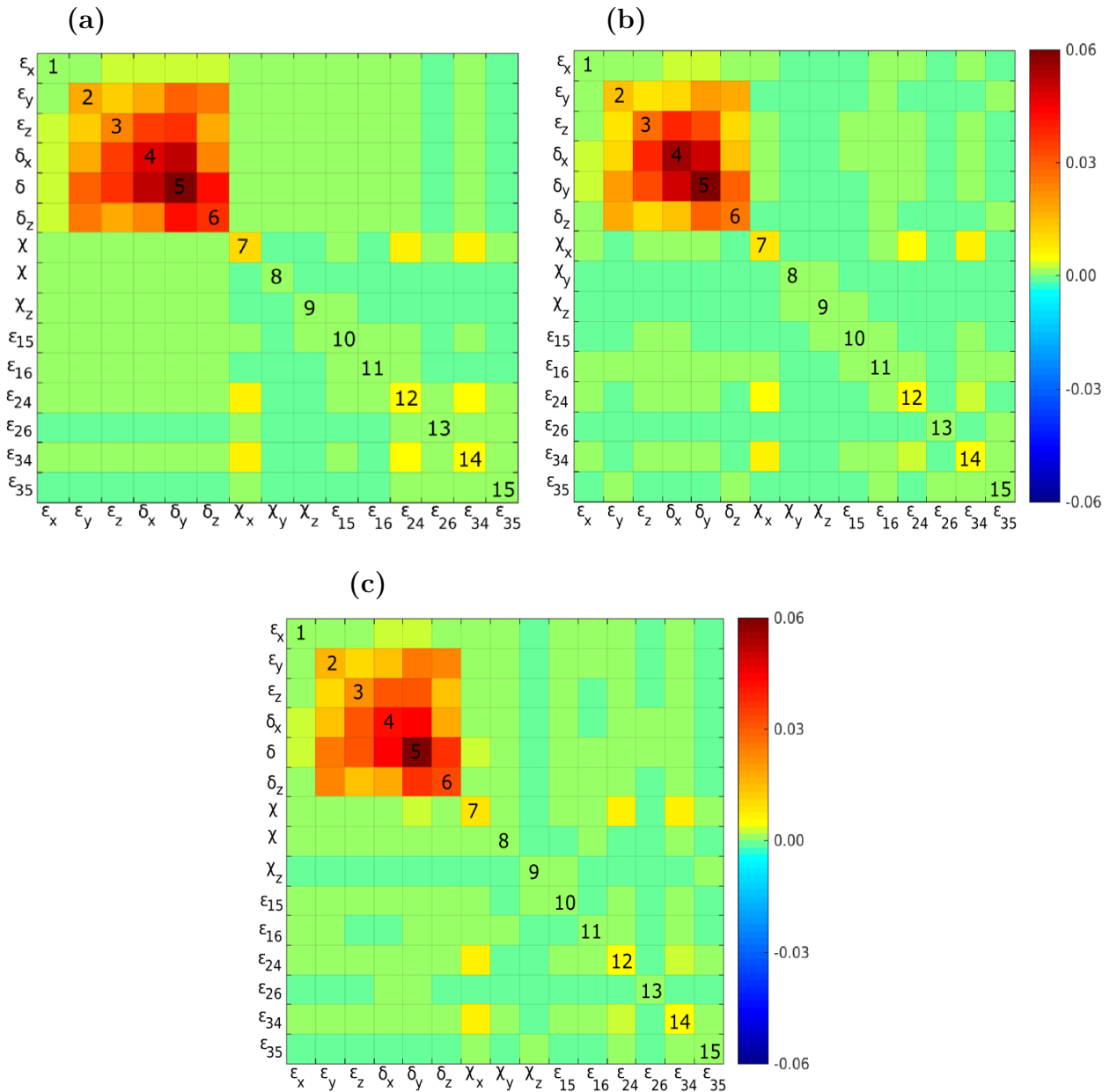


Figure 4.10: Model covariance matrices computed for experiments using the three acquisition geometries to the receiver in the horizontal borehole. (a) For sources along 5 profiles. (b) For random sources. (c) For spiral sources pattern.

Figure 4.11 shows the stereographic maps of phase velocity computed using exact WA parameters (Figure 4.11a), using estimated parameters from data generated by sources along five profiles (Figure 4.11b), randomly distributed (Figure 4.11c) and in spiral pattern (Figure 4.11d), and the stereographic projection of percentage error between estimated maps and the exact one (Figure 4.11e, Figure 4.11f and Figure 4.11g). Comparing the results, it is observed that estimated phase velocities and percentage error are similar for the three source distributions. Note that error does not exceed 1.5%. As mentioned, the model used exhibits anisotropy strength about 8%, so we consider that the phase velocities are well estimated for error below 4%.

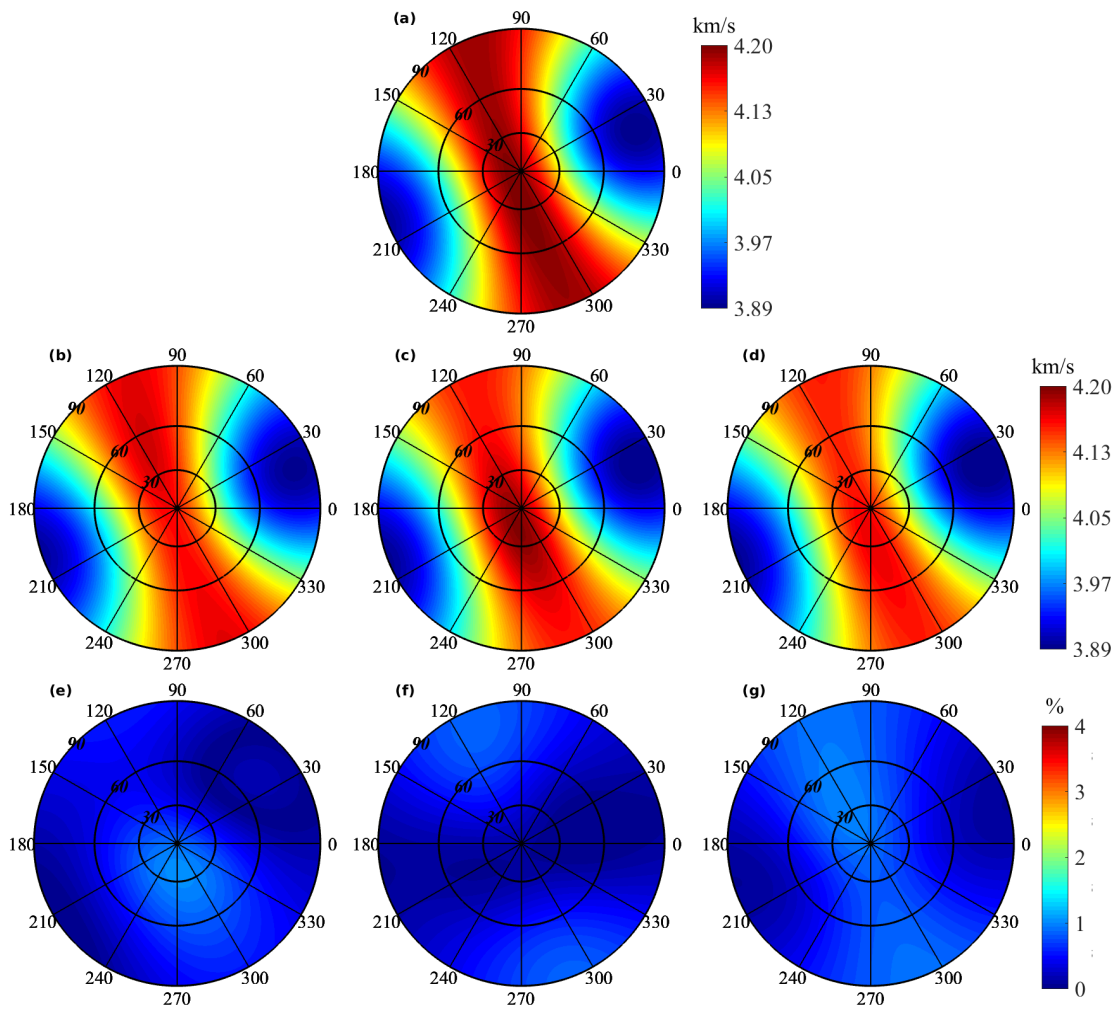


Figure 4.11: Stereographic maps to the receiver in the horizontal borehole. (a) Phase velocity computed using exact WA parameters. (b) Phase velocity computed using estimated WA parameter for experiment with sources distributed along five profiles. (c) Phase velocity computed using estimated WA parameter for experiment with sources distributed randomly. (d) Phase velocity computed using estimated WA parameter for experiment with sources distributed in spiral pattern. (e) Percentage error between (a) and (b). (f) Percentage error between (a) and (c). (g) Percentage error between (a) and (d).

Figure 4.12 shows percentage variation maps of phase velocity. It is obtained from phase velocity computed using the parameters estimated from 500 simulations. The results for sources distributed along five profiles, randomly and in spiral pattern are shown in Figure 4.12a, Figure 4.12b and Figure 4.12c, respectively. According to these figures, it is observed that the phase velocity suffers less variation around the x -axis. As elevation angle increases the velocity variation also increases. Here, instead of the polar angle, which is measured from a z -axis direction, we use elevation angle, which is measured from a x -axis direction. Thus, the best estimates are obtained within the region delimited by a 30° cone around the wellbore direction. Comparing the results for the three sources geometries, we note that the variation is similar for the three experiments.

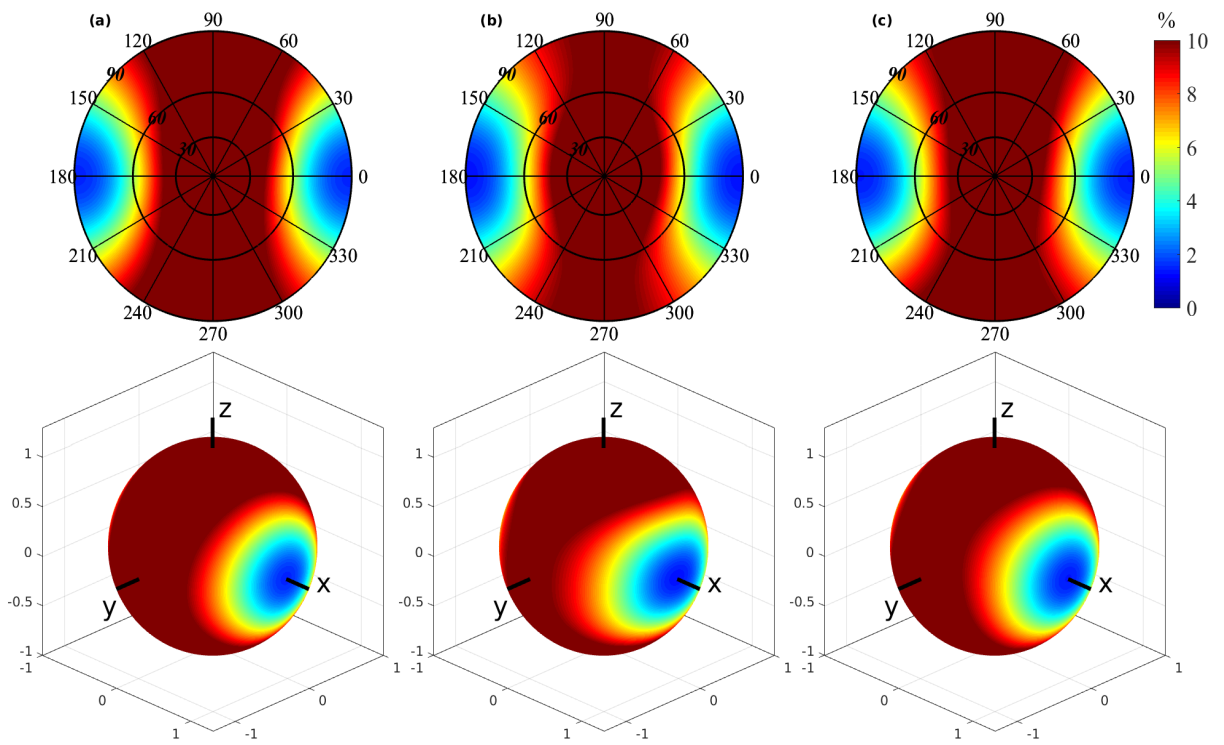


Figure 4.12: Percentage variation maps (stereographic projections and its corresponding spherical surfaces) of phase velocity to the receiver in the horizontal borehole. (a) Results for sources along 5 profiles. (b) Results for sources distributed randomly. (c) Results for sources distributed in spiral pattern.

5 DISCUSSION

Linearized inversion equation for qP -wave recorded in vertical borehole have been tested by real walkaway VSP data (Gomes et al., 2004) and by synthetic multiazimuthal walkaway VSP data (Barreto et al., 2013; Macambira et al., 2014). In this work, we have investigated the use of sources distributed randomly and in spiral pattern for anisotropy estimation. In performed tests, we compare the results obtained with data generated by these two types of source distribution with the result obtained from sources distributed along five radial profiles, which is the geometry used in Barreto et al. (2013). Furthermore, we also addressed the problem of inversion of VSP qP -wave data recorded in horizontal borehole.

The model covariance matrix can provide a general insights into how the survey geometry influences the parameters estimation. In the tests performed with synthetic data obtained within vertical borehole, for the shallower receiver (located at 0.1 km depth), the error propagation and uncertainty in the parameters estimates are greater when is used sources distributed in spirals pattern and smaller for distribution along five radial profiles, whereas for the deeper receiver (located at 0.5 km depth) the matrices computed for the three geometries are similar. This difference is believed to be due to worst ray coverage provided by sources distributed randomly and in spiral pattern in shallow depth. In the experiment with horizontal borehole, the receiver is also located at 0.5 km depth. In this case, the results obtained for the three survey designs are similar. Additionally, results shows that the computed covariance matrix are consistent with the corresponding percentage variation map of phase velocity. That is, the larger the error amplification in the matrix, the greater the variation of the estimated phase velocities.

In contrast to study of Ruzek and Pšenčík (2016), here no advantages were observed in the use of randomly distributed sources on the surface. In the method presented in Ruzek and Pšenčík (2016), the estimation of the WA parameters is made from traveltime measurements, in addition the anisotropic medium used is homogeneous, which enables the inversion of data from multiple receivers together. While in the method presented in this study is used measurements of polarization and slowness, further the medium is heterogeneous and the inversion is performed for each receiver. Therefore, for the model and method used in this work the use of randomly source distribution does not improve the parameters estimation.

The limited illumination of the medium together with the presence of noise in the data reduce the number of resolvable WA parameters. For data recorded in vertical borehole, seven parameters are accurately estimated: ϵ_z , χ_x , χ_y , ϵ_{15} , ϵ_{24} , ϵ_{34} and ϵ_{35} . This is because these parameters are related to vertical propagation, that is, to the component n_3 of wave normal vector n_i (see Eq. 2.12, Eq. 2.13 and Eq. 2.14). These results are in agreement

with previous works (Barreto et al., 2013; Macambira et al., 2014). For data recorded in horizontal borehole, seven parameters are also well estimated: ϵ_x , χ_y , χ_z , ϵ_{15} , ϵ_{16} , ϵ_{26} and ϵ_{35} . In this case, the parameters are related to horizontal propagation in the x direction, that is, to the component n_1 (see Eq. 2.12, Eq. 2.13 and Eq. 2.14). Note that three WA parameters (χ_y , ϵ_{15} and ϵ_{35}) are accurately estimated for the two wellbore configuration, this is because they are related to both components n_3 and n_1 .

The stability of estimated phase velocities is determined by computation of percentage variation maps. Thus, the phase velocities are considered well estimated in the vicinity of the receiver for angles within about 30° from the borehole direction. This is because these portions of phase velocity surface are prevalingly controlled by the seven WA parameters which are accurately recovered for each wellbore configuration.

Therefore, for the case of vertical borehole configuration, the phase velocities within 30° cone around z -axis depends mostly on the parameter ϵ_z , which are related to the elastic parameter A_{33} (see Equation 2.9). This value is about the square of the qP -wave velocity in vertical direction. While for horizontal borehole configuration, the phase velocities within 30° cone around x -axis depends mainly on the parameter ϵ_x , which are related to the elastic parameter A_{11} (see Equation 2.9). This value is about the square of the qP -wave velocity in horizontal direction given by x -axis. These results are in agreement with previous studies regarding the inversion scheme for vertical wellbore (Barreto et al., 2013; Macambira et al., 2014). Thus, in this work, we verified that the results are analogous to inversion scheme considering the horizontal wellbore.

For VSP experiments with vertical borehole we used 90 sources and measurements of direct and reflected qP -wave. Whereas for experiments with horizontal borehole we used 180 sources and only measurements of direct qP -wave. The use of reflected data adds more observations than those provided only by direct data, besides that, by employing the reflected wave together with direct wave, the polar illumination aperture is increased (Gomes et al., 2004; Rusmanugroho and McMechan, 2012). For this reason, in the experiments with horizontal borehole we used twice the number of sources employed in the experiments with vertical borehole configuration and we also extend the source offsets.

6 CONCLUSION

Measurements of slowness and polarization obtained from VSP surveys allow estimation of local anisotropy in subsurface. Here, the inversion procedure is based on a linearized model that relates weak anisotropy (WA) parameters of the medium around a borehole receiver to measurements of polarization and slowness of qP-wave recorded in the receiver. In the procedure is used the three components of the polarization and only the slowness component along the receiver array, therefore it is independent of the complexity of the overburden. This approach has already been applied in previous works for data recorded within vertical borehole.

In the present work we derived a linear equation model that can be used for inversion of data recorded within a horizontal borehole, in this situation the observations comprises the polarization vector and the horizontal slowness component in well direction. The proposed equation was tested in synthetic datasets.

Numerical tests were performed for synthetic data recorded in vertical and horizontal borehole. The results shows that seven WA parameters can accurately estimated for both wellbore configuration. The estimates were evaluated by computing the model covariance matrix and the phase velocity. For vertical borehole configuration, the well estimated parameters are related to the near vertical propagation: ϵ_z , χ_x , χ_y , ϵ_{15} , ϵ_{24} , ϵ_{34} and ϵ_{35} . While for horizontal borehole configuration, the accurately estimated parameters are related to horizontal propagation in the direction of borehole: ϵ_x , χ_y , χ_z , ϵ_{15} , ϵ_{16} , ϵ_{26} and ϵ_{35} .

According to inversion results, the qP -wave phase velocities are well estimated for angles within about 30° from the borehole direction. Therefore, for VSP data acquired in a vertical wellbore the estimated phase velocities delimited by a 30° cone around vertical axis are governed by the seven resolvable WA parameters, mainly by ϵ_z , related to elastic parameter A_{33} which is about the square of the qP -wave velocity in vertical direction. In an analogous way, for data acquired in the horizontal wellbore the estimated phase velocities delimited by a 30° cone around the horizontal borehole direction are governed by the seven accurately recovered parameters, mainly by ϵ_x , related to elastic parameter A_{11} which is about the square of the qP -wave velocity in x -axis direction.

We also investigated the use of different types of source distribution on the surface. In the tests, we considered three types of acquisition geometry: sources along five radial profiles, randomly distributed and in spiral pattern for either vertical and horizontal borehole configuration. The model covariance matrix is a useful tool to evaluate the sensitivity of the inversion scheme with respect to survey design. The numerical experiments showed that in some cases one of these source distribution can produce a larger error in estimated model parameters in comparison with another one, which is consequence of different

illumination of the medium provided for each source-receiver geometry. Nonetheless, we believe that, in general, the use of all three investigated source distributions will yield similar results. Furthermore, regarding to seven WA parameters that are well estimated for both borehole configurations, it is noteworthy that they are accurately determined from data generated by the three distributions of sources.

REFERENCES

- Asgharzadeh, M., Bóna, A., Pevzner, R., Urosevic, M. and Gurevich, B., 2013, Reliability of the slowness and slowness-polarization methods for anisotropy estimation in VTI media from 3C walkaway VSP data. *Geophysics*, **78**(5), WC93–WC102, doi:10.1190/geo2012-0409.1.
- Aster, R.C., Borchers, B. and Thurber, C.H., 2011, Parameter estimation and inverse problems, vol. 90. Academic Press.
- Barreto, A., Gomes, E.N., Macambira, R.N. and Costa, J.C., 2013, Improvement of local anisotropy estimation from VSP data through experimental design. *Journal of Geophysics and Engineering*, **10**(4), doi:10.1088/1742-2132/10/4/045008.
- Dewangan, P. and Grechka, V., 2003, Inversion of multicomponent, multiazimuth, walkaway VSP data for the stiffness tensor. *Geophysics*, **68**(3), 1022–1031, doi:10.1190/1.1581073.
- Farra, V. and Pšenčík, I., 2003, Properties of the zeroth-, first-, and higher-order approximations of attributes of elastic waves in weakly anisotropic media. *The Journal of the Acoustical Society of America*, **114**(3), 1366–1378.
- Gaiser, J., 1990, Transversely isotropic phase velocity analysis from slowness estimates. *Journal of Geophysical Research: Solid Earth*, **95**(B7), 11241–11254.
- Gajewski, D. and Pšenčík, I., 1990, Vertical seismic profile synthetics by dynamic ray tracing in laterally varying layered anisotropic structures. *Journal of Geophysical Research: Solid Earth*, **95**(B7), 11301–11315.
- Gomes, E., Zheng, X., Pšenčík, I., Horne, S. and Leaney, S., 2004, Local Determination of Weak Anisotropy Parameters from Walkaway VSP qP-Wave Data in the Java Sea Region. *Studia Geophysica et Geodaetica*, **48**(1), 215–231, doi:10.1023/B:SGEG.0000015593.29477.88.
- Grechka, V. and Mateeva, A., 2007, Inversion of P-wave VSP data for local anisotropy: Theory and case study. *Geophysics*, **72**(4), D69–D79, doi:10.1190/1.2742970.
- Horne, S. and Leaney, S., 2000, Short note: Polarization and slowness component inversion for TI anisotropy. *Geophysical Prospecting*, **48**(4), 779–788, doi:10.1046/j.1365-2478.2000.00205.x.
- Jílek, P., Hornby, B. and Ray, A., 2003, Inversion of 3D VSP P-wave data for local anisotropy: A case study. In: *SEG Technical Program Expanded Abstracts 2003*. Society of Exploration Geophysicists, 1322–1325.

- Macambira, R.N.A., Gomes, E.N.S. and Barreto, A.C.R., 2014, Analysis of a linear scheme for estimation of local anisotropy from P-wave data in multi-azimuth VSP surveys. *Revista Brasileira de Geofísica*, **32**(4), 707–720.
- Menke, W., 2012, *Geophysical data analysis: discrete inverse theory: MATLAB edition*, vol. 45. Academic press.
- Miller, D.E. and Spencer, C., 1994, An exact inversion for anisotropic moduli from phase slowness data. *Journal of Geophysical Research: Solid Earth*, **99**(B11), 21651–21657.
- Parscau, J., 1991, P-and SV-wave transversely isotropic phase velocities analysis from VSP data. *Geophysical Journal International*, **107**(3), 629–638.
- Pšenčík, I. and Gajewski, D., 1998, Polarization, phase velocity, and nmo velocity of qp-waves in arbitrary weakly anisotropic media. *Geophysics*, **63**(5), 1754–1766.
- Rusmanugroho, H. and McMechan, G., 2012, Sensitivity of estimated elastic moduli to completeness of wave type, measurement type, and illumination apertures at a receiver in multicomponent VSP data. *Geophysics*, **77**(1), R1–R18, doi:10.1190/geo2010-0410.1.
- Ruzek, B. and Pšenčík, I., 2016, P-wave VSP travelttime inversion in weakly and moderately anisotropic media. *Seismic Waves in Complex 3-D Structures*, **26**, 17–59.
- Thomsen, L., 1986, Weak elastic anisotropy. *Geophysics*, **51**(10), 1954–1966.
- Tsvankin, I. and Grechka, V., 2011, *Seismology of azimuthally anisotropic media and seismic fracture characterization*. Society of Exploration Geophysicists.
- Zheng, X. and Pšenčík, I., 2002, Local Determination of Weak Anisotropy Parameters from qP-wave Slowness and Particle Motion Measurements. *Pure and Applied Geophysics*, **159**(7-8), 1881–1905.